
Article:
De Domenico, D., Askes, H. orcid.org/0000-0002-4900-1376 and Aifantis, E.C. (2018) Gradient elasticity and dispersive wave propagation: Model motivation and length scale identification procedures in concrete and composite laminates. International Journal of Solids and Structures. ISSN 0020-7683

https://doi.org/10.1016/j.ijsolstr.2018.09.007

International Journal of Solids and Structures 000 (2018) 1–15

Contents lists available at ScienceDirect

International Journal of Solids and Structures

journal homepage: www.elsevier.com/locate/ijsolstr

Gradient elasticity and dispersive wave propagation: Model motivation and length scale identification procedures in concrete and composite laminates

Dario De Domenico[a,*], Harm Askes[b], Elias C. Aifantis[c,d]

[a] Department of Engineering, University of Messina, Contrada Di Dio, Sant'Agata, Messina 98166, Italy
[b] Department of Civil and Structural Engineering, University of Sheffield, Mappin Street, Sheffield S1 3JD, UK
[c] Laboratory of Mechanics and Materials, Aristotle University of Thessaloniki, Thessaloniki 54006, Greece
[d] Michigan Technological University, Houghton, MI 49931, USA

ARTICLE INFO

Article history:
Received 1 February 2018
Revised 30 July 2018
Available online xxx

Keywords:
Wave dispersion
Gradient elasticity
Internal length scale
Concrete
Layered composites
Micro-structural effects
Length scale identification
Micro-structural effects
Analytical solutions

ABSTRACT

Nano-scale experimental findings reveal that wave propagation in heterogeneous materials is dispersive. In order to capture such dispersive behavior, in this paper gradient elasticity theory is resorted to. A popular gradient elasticity model arising from Mindlin's theory incorporates two internal length scale parameters, which correspond to one micro-stiffness and one micro-inertia term. As an extension of Mindlin's model, an expanded *three-length-scale* gradient elasticity formulation with one additional micro-inertia term is used to improve the description of microstructural effects in dynamics. A non-local lattice model is introduced here to give the above micro-stiffness and micro-inertia terms a physical interpretation based on geometrical and mechanical properties of the microstructure. The purpose of this paper is to assess the effectiveness of such a three-length-scale formulation in predicting wave dispersion against *experimental and micro-mechanical data* from the literature. The dispersive wave propagation through laminated composites with periodic microstructure is investigated first. Length scale identification is carried out based on higher-order homogenization to link the constitutive coefficients of the gradient theory directly to microstructural properties of the layered composite. Secondly, experimental dispersion curves for phonons propagating in aluminum and bismuth crystals are scrutinized, thus highlighting the motivation for including *multiple micro-inertia terms*. Finally, ultrasonic wave dispersion experimentally observed in concrete specimens with various sand contents and water/cement ratios is analyzed, along with length scale quantification procedures. It is found that the proposed three-length-scale gradient formulation is versatile and effective in capturing a range of wave dispersion characteristics arising from experiments. Advantages over alternative formulations of gradient elasticity from the literature are discussed throughout the paper.

1. Introduction

Classical (local) elasticity theory fails to describe those physical phenomena in which non-local (long-range) interactions play a major role in the deformation process. This occurs in materials with a lattice microstructure and heterogeneous media wherein the external length-scales and time-scales are of the same order as those of the dominant heterogeneities. Among the physical phenomena not captured by the classical theory of elasticity, of particular relevance to the present paper is the *dispersion* observed in the wave propagation (Askes and Aifantis, 2011). Indeed, experimental evidence points out that the different harmonic wave components travel with different velocities (Warren et al., 1967; Yarnell et al., 1964a,b, 1965; Aggelis et al., 2005; Philippidis and Aggelis, 2005). These dispersive phenomena cannot be captured unless long-range interactions, occurring within the material microstructure, are accounted for in the constitutive model. One obvious solution could be modeling every single microstructural component individually, which represents the basis of molecular/atomistic models. Nevertheless, such models may be computationally prohibitive or extremely demanding on memory resources, thus unfeasible to cope with real engineering problems. As an al-

* Corresponding author.
E-mail address: dario.dedomenico@unime.it (D. De Domenico).

https://doi.org/10.1016/j.ijsolstr.2018.09.007

ternative, nonlocal continuum field theories (Eringen, 1983; Fuschi et al., 2015; Polizzotto et al., 2006) and higher-order continuum theories (Maugin and Metrikine, 2010), including gradient elasticity (Askes and Aifantis, 2011; Mindlin, 1964; Aifantis 1992; Altan and Aifantis 1997; Bažant and Jirásek, 2002), have been developed to bridge the gap between atomistic models and classical continuum mechanics theory.

In particular, *gradient elasticity* formulations enrich the field equations of classical elasticity theory by means of additional higher-order spatial derivatives of relevant state variables (such as strains, stresses and/or accelerations). These higher-order terms are accompanied by length scale parameters, which reflect the underlying material microstructure. An effective class of gradient elasticity theories for use in dynamics involves mixed spatial–temporal derivatives by incorporating higher-order contributions both in the stiffness terms and in the inertia terms (Askes and Aifantis, 2006; Metrikine and Askes, 2002, 2006; Askes and Metrikine, 2002; Askes et al., 2007; Papargyri-Beskou et al., 2009; Askes et al., 2008). While inclusion of the Laplacian of the strain in the constitutive relation is essential to remove singularities from the elastic strain field, the acceleration gradients (micro-inertia terms) are of paramount importance to capture the dispersive character of the wave propagation. The role of micro-inertia in enriched continuum theories has been recently investigated in the field of metamaterials (Madeo et al., 2017).

Along this research line, a new three-length-scale gradient formulation has been developed recently by the authors (De Domenico and Askes, 2016, 2017). In addition to Aifantis' gradient elasticity (Aifantis, 1992; Altan and Aifantis, 1997; Ru and Aifantis, 1993; Triantafyllidis and Aifantis, 1986) the new model incorporates *two micro-inertia terms* multiplying the second-order and the fourth-order space derivative of the acceleration field in the equations of motions. This model is very versatile and provides an improved dispersion behavior due to the presence of the two micro-inertia terms, as previously shown in (De Domenico and Askes, 2016).

A first novel contribution of the present paper is to provide some micro-mechanical background to the model with three length scales. In order to correlate the three length scale parameters with the material microstructure, a non-local *lattice model* is presented, based on the standard "continualization" of the equations of motion involving both lumped and distributed mass terms. In this way, all three length scale parameters can be assigned a physical meaning based on geometrical and mechanical properties of the microstructure.

The next aim of this paper is to assess the dispersive capabilities of the proposed formulation by addressing a few experimental dispersion curves reported in the literature. The longitudinal wave dispersion in a bi-layered composite laminate with periodic microstructure, which has been widely discussed in the relevant literature (Ruzzene and Baz, 2000; Bennett et al., 2007; Andrianov et al., 2008, 2011a,b; Chen and Fish, 2001; Fish et al., 2002; Dontsov et al., 2013), is first examined. Length scale identification is carried out based on asymptotic higher-order homogenization (Fish and Chen, 2001), so as to link the three constitutive coefficients of the gradient elasticity theory directly to microstructural properties of the composite laminate. The exact dispersion curve (Bedford and Drumheller, 1994) is approximated closely by the proposed three-length-scale gradient elasticity formulation. Physically-based (pseudo-experimental) results are also simulated via the spectral analysis of surface waves (SASW) (Kim and Park, 2002) in conjunction with the phase spectrum approach (Sachse and Pao, 1978) and compared to the ones provided by the gradient elasticity model. Next, longitudinal dispersion curves of phonons propagating in aluminum and bismuth are investigated (Warren et al., 1967; Yarnell et al., 1964a,b, 1965). It is seen that the inclusion of the fourth-order acceleration gradient is essential to capture the qualitative trend of such dispersion curves, which exhibit an inflexion in the medium wave number regime that cannot be captured with a single micro-inertia term. Finally, the dispersive behavior of ultrasonic wave propagation in fresh mortar and hardened concrete specimens having various water and sand contents is analyzed (Aggelis et al., 2005; Philippidis and Aggelis, 2005; Iliopoulos et al., 2016), and corresponding length scale quantification procedures presented.

Throughout the paper alternative, simpler formats of gradient elasticity theories presented in the literature, equipped with one or two length scales, are retrieved as special cases of the three-length-scale formulation here proposed.

Incidentally, the proposed formulation not only improves the dispersive behavior, but also is particularly appealing from a computational point of view for straightforward numerical implementation. Indeed, the authors have demonstrated that this particular format of gradient elasticity can be handled, via an operator split, such that a finite element implementation with simple linear shape functions is possible (De Domenico and Askes, 2017), thus avoiding the need for more sophisticated discretization techniques (Askes and Metrikine, 2002; Zervos et al., 2009; Engel et al., 2002; Zervos, 2008).

2. Three-Length-Scale gradient elasticity theory

Motivated by nano-scale experimental evidence on the dispersion characteristics of materials with a lattice structure (Warren et al., 1967; Yarnell et al., 1964a,b, 1965), a new gradient elasticity formulation with three higher-order terms has been proposed in (De Domenico and Askes, 2016, 2017). In particular, it includes one strain gradient (Aifantis' term corresponding to the Laplacian of the strain field) and two micro-inertia contributions. The starting point is the following constitutive equation

$$\sigma_{ij} = C_{ijkl}\left(\varepsilon_{kl} - \ell_1^2 \varepsilon_{kl,nn} + \ell_2^2 \ddot{\varepsilon}_{kl} - \ell_3^4 \ddot{\varepsilon}_{kl,nn}\right) \tag{1}$$

where, for reasons of dimensional consistency, the three gradient terms are accompanied by three distinct length-scale factors ℓ_1, ℓ_2, ℓ_3. More specifically, these terms relate essentially to internal lengths and internal times, i.e., expanding ε_{kl} in Taylor series not only in space but also in time. This is more simply demonstrated via the one-dimensional format of Eq. (1) that reads

$$\sigma = E\left(\varepsilon - \ell_1^2 \varepsilon'' + \ell_2^2 \ddot{\varepsilon} - \ell_3^4 \ddot{\varepsilon}''\right) \tag{2}$$

where E is the Young's modulus, and overdots and primes are adopted for derivatives with respect to time and to the spatial coordinate x, respectively. Eq. (2) may be rewritten as

$$\begin{aligned} &\sigma = E\tilde{\varepsilon} \\ &\tilde{\varepsilon} = \left(1 - \ell_1^2 \nabla_x^2 + \ell_2^2 \nabla_t^2 - \ell_3^4 \nabla_x^2 \nabla_t^2\right)\varepsilon \quad \text{with } \nabla_x^2 = \tfrac{\partial^2}{\partial x^2},\ \ \nabla_t^2 = \tfrac{\partial^2}{\partial t^2}. \end{aligned} \tag{3}$$

Considering the equilibrium equation $\sigma' - \rho\ddot{u} = 0$, after rearranging terms, we get the following equation of motion in terms of displacements

$$\rho\left(\ddot{u} - \frac{E}{\rho}\ell_2^2 \ddot{u}'' + \frac{E}{\rho}\ell_3^4 \ddot{u}''''\right) = E\left(u'' - \ell_1^2 u''''\right) \tag{4}$$

which, to make the notation consistent with the quoted papers (De Domenico and Askes, 2016, 2017), may be rewritten as

$$\rho\left(\ddot{u} - \alpha\ell^2 \ddot{u}'' + \beta\ell^4 \ddot{u}''''\right) = E\left(u'' - \gamma\ell^2 u''''\right) \tag{5}$$

in which the three length scales ℓ_1, ℓ_2, ℓ_3 have been reported in terms of just a single length scale parameter ℓ characterizing the underlying material microstructure. The three dimensionless coefficients α, β, γ adjust the relative magnitudes between the various length scales appearing in the strain gradient term and in

Please cite this article as: D. De Domenico et al., Gradient elasticity and dispersive wave propagation: Model motivation and length scale identification procedures in concrete and composite laminates, International Journal of Solids and Structures (2018), https://doi.org/10.1016/j.ijsolstr.2018.09.007

the micro-inertia contributions. More specifically, the $\gamma\ell^2$ term represents the gradient enrichment of the strain gradient theory (Aifantis, 1992), whereas the higher-order inertia contributions multiply two additional length scale factors $\alpha\ell^2$ and $\beta\ell^4$, respectively. Therefore, higher-order contributions appear simultaneously as micro-stiffness and micro-inertia, which has been termed as *dynamic consistency* in a few previous articles (Askes and Aifantis, 2006, 2011; Metrikine and Askes 2002, 2006; Askes et al., 2007). The simplest dynamically consistent model incorporating one micro-inertia term $\alpha\ell^2$ and one micro-stiffness term $\gamma\ell^2$ has been extensively used in the relevant literature, see e.g. (Askes and Aifantis, 2006, 2011; Askes et al., 2007; Papargyri-Beskou et al., 2009; Polyzos and Fotiadis 2012; Dontsov et al., 2013; Ansari et al., 2012; Iliopoulos et al., 2016) to quote just a few. As compared to this model, there is an additional $\beta\ell^4$ term in the proposed formulation, which improves the prediction of wave dispersion and allows for greater flexibility in terms of shape of the corresponding dispersion curve, as demonstrated in the next Sections.

The dispersion behavior of Eq. (5) can be described by the following dimensionless expressions

$$\left(\frac{\omega\ell}{c_e}\right)^2 = (k\ell)^2\,\frac{1+\gamma(k\ell)^2}{1+\alpha(k\ell)^2+\beta(k\ell)^4}$$
$$\left(\frac{c}{c_e}\right)^2 = \frac{1+\gamma(k\ell)^2}{1+\alpha(k\ell)^2+\beta(k\ell)^4} \tag{6}$$

where $c_e \equiv \sqrt{E/\rho}$ is the one-dimensional wave velocity of classical elasticity, ω is the angular frequency, k the wave number and $c=\omega/k$ the phase velocity.

As a remark, it is worth noting that the inertia-gradient terms in Eq. (5) lead to non-classical gradient-dependent inertia terms in the equation of motion, i.e. in the left-hand-side of Eq. (5) – the last two terms. These non-classical terms, in analogy to the first classical inertia term of this equation, introduce gradient-dependent Coriolis force effects (see, for example, (Truesdell and Toupin, 1960; Truesdell and Noll, 2004)) under a change of frame. In fact, the aforementioned two non-classical gradient dependent terms may be viewed as representing coupling effects between internal lengths and internal times/lags of the underlying micro/nano structures (see, for example (Aifantis 2016)).

3. Physical background of the three length scale gradient model

In many studies, gradient elasticity theories have been derived from the continualization of the response of a discrete lattice, see e.g. (Metrikine and Askes, 2002, 2006; Askes et al., 2008; De Domenico and Askes, 2016; Polyzos and Fotiadis, 2012; Chang and Gao, 1995). In an attempt to provide a theoretical background of the proposed gradient formulation, two motivations for the model are provided in this Section. First, we will suggest a novel approach to continualization of a lattice. Next, we will present a derivation based on Hamilton's principle. Perhaps neither of these two motivations should be considered as definitive or as superior over the other, but they are included here and presented alongside one another in the hope to trigger constructive debate and discourse in the community.

3.1. A novel multi-scale approach to homogenization of a discrete lattice

First, a clear physical meaning depending on the underlying material microstructure is provided by a novel approach to homogenization of discrete mass at multiple scales of observation. A simple lattice model is given in Fig. 1.

We consider a material in which, at the macro level, a portion of the mass is distributed and the remainder is lumped. This material is schematically represented by a chain of mass particles having mass M being connected to each other by springs of stiffness k and with distributed mass ρ_m. Uniform spacing of the lumped mass particles is assumed to be equal to ℓ, which is hence meant as the unit cell of the non-homogeneous material. The physical motivation for distributed mass at the macro level is to interpret this distributed mass as a macro-level representation of lumped masses at the micro level. Such additional micro-mass distribution is represented by another discrete set of smaller masses m_e that are placed in between two neighbor particles M, i.e., within the unit cell ℓ, and are connected with each other through springs of stiffness k_e, cf. again Fig. 1. This additional micro-distribution of mass and stiffness in series is equivalent to $\rho_m A\ell = m$ and $\Sigma 1/k_e = 1/k$. From another perspective, the springs k characterizing the connections of the chain at the macroscale are not considered massless as in classical lattice model, but springs with uniformly distributed mass m and density ρ_m (micro-volume density) (Polyzos and Fotiadis, 2012). It is this micro-mass distribution that is responsible for the higher-order terms of the proposed gradient elasticity formulation, as will be explained below.

The various discrete model properties can be translated into continuum properties in the usual way. In particular, the continuous counterpart of the lumped mass at macro level and the stiffness of the material are the macroscale mass density $\rho_M = M/A\ell$, and the Young's modulus $E = k\ell/A$, with A denoting the cross-sectional area, in addition to the microscale mass density $\rho_m = \Sigma m_e/A\ell$ as defined above.

In an attempt to write the equation of motion of the n^{th} degree of freedom (located at x_n), we introduce the stiffness matrix of the unit cell, which has the well-known expression

$$\mathbf{K} = \begin{bmatrix} k & -k \\ -k & k \end{bmatrix}. \tag{7}$$

For the mass matrix representation, we need to distinguish the two contributions. A standard lumped mass matrix can be used for the lumped mass particles M of the macro level. On the other hand, the lumped mass particles of the micro-level have been translated to a distributed mass at the macro level, for which a so-called consistent mass matrix is more appropriate to represent this contribution. Thus, we adopt

$$\mathbf{M}_{\text{micro}} = \frac{\rho_m A\ell}{6}\begin{bmatrix} 2 & 1 \\ 1 & 2 \end{bmatrix}; \qquad \mathbf{M}_{\text{macro}} = \frac{M}{2}\begin{bmatrix} 1 & 0 \\ 0 & 1 \end{bmatrix}. \tag{8}$$

whereby the consistent mass matrix of the first expression is based on a linear resolution of the displacement field, which is in accordance with the resolution underlying Eq. (7) – see for instance standard finite element textbooks (Hughes, 2000). With the stiffness and mass matrices introduced, the generic n^{th} particle must satisfy the following equation

$$M\ddot{u}_n + \frac{\rho_m A\ell}{6}(\ddot{u}_{n-1} + 4\ddot{u}_n + \ddot{u}_{n+1}) + k(-u_{n-1} + 2u_n - u_{n+1}) = 0. \tag{9}$$

Now, continualization is performed by translating the response of the discrete particle u_n into the continuous displacement $u(x)$, cf. Fig. 1. For the neighboring particles, this means $u_{n\pm1} = u(x \pm \ell)$ because $x_{n\pm1} = x_n \pm \ell$. The continuous counterpart of Eq. (9) is

$$\rho_M A\ell\,\ddot{u}(x) + \frac{\rho_m A\ell}{6}(\ddot{u}(x-\ell) + 4\ddot{u}(x) + \ddot{u}(x+\ell)) = \frac{EA}{\ell}(u(x-\ell) - 2u(x) + u(x+\ell)). \tag{10}$$

Please cite this article as: D. De Domenico et al., Gradient elasticity and dispersive wave propagation: Model motivation and length scale identification procedures in concrete and composite laminates, International Journal of Solids and Structures (2018), https://doi.org/10.1016/j.ijsolstr.2018.09.007

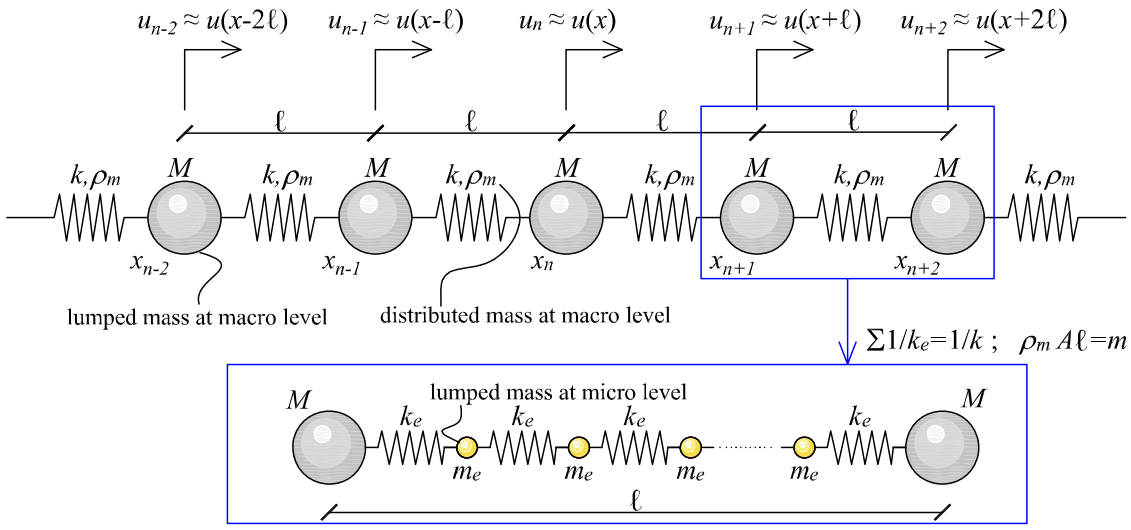

Fig. 1. Lattice with both distributed and lumped mass.

By using Taylor expansions for the $u(x \pm \ell)$ and $\ddot{u}(x \pm \ell)$ terms, after some straightforward algebra Eq. (10) can be rewritten as

$$(\rho_M + \rho_m)\,\ddot{u}(x) + \frac{\rho_m \ell^2}{6}\left(\ddot{u}''(x) + \frac{\ell^2}{12}\ddot{u}''''(x) + \frac{\ell^4}{360}\ddot{u}''''''(x)\right) = E\left(u''(x) + \frac{\ell^2}{12}u''''(x) + \frac{\ell^4}{360}u''''''(x)\right) + \mathcal{O}(\ell^6) \tag{11}$$

The expansion terms in Taylor series are truncated in order to make Eq. (11) asymptotically accurate up to $\mathcal{O}(\ell^6)$. Omitting the space dependence of the displacement, that is, $u = u(x)$, and introducing the so-called "total density" $\rho = \rho_m + \rho_M$ leads to the following compact equation

$$\rho\,\ddot{u} = \left(1 + \frac{\ell^2}{12}\nabla_x^2 + \frac{\ell^4}{360}\nabla_x^4 + \ldots\right)\left(Eu'' - \frac{1}{6}\ell^2\rho_m\ddot{u}''\right) \tag{12}$$

from which we notice that higher-order inertia gradients are uniquely ascribed to the presence of the micro-mass distribution ρ_m. Within the gradient series, the 2nd term is unstable and incorrect in the Garding sense (Filimonov, 1996), while the 3rd term is correct and stable (Andrianov et al., 2010). Thus, loss of stability is not a primary concern, and Eq. (12) could be used effectively. Nevertheless, in order to aid parameter identification in Eq (5), we apply Padé approximation of the differential operator, that is

$$\left(1 + \frac{\ell^2}{12}\nabla^2 + \frac{\ell^4}{360}\nabla^4 + \ldots\right) \approx \frac{1}{\left(1 - \frac{\ell^2}{12}\nabla^2 + \frac{\ell^4}{240}\nabla^4 + \ldots\right)} \tag{13}$$

so that Eq. (12) is rewritten as

$$\left(1 - \frac{\ell^2}{12}\nabla^2 + \frac{\ell^4}{240}\nabla^4 + \ldots\right)\rho\,\ddot{u} = Eu'' - \frac{1}{6}\ell^2\rho_m\ddot{u}'' \tag{14}$$

which can be shown to be stable. The negative term on the right-hand-side can also be expressed in terms of an equivalent higher-order strain gradient plus an additional fourth-order inertia gradient term: from (14) we get

$$\ddot{u} = \frac{E}{\rho}u'' + \frac{1}{12}\left(\frac{\rho - 2\rho_m}{\rho}\right)\ell^2\ddot{u}'' + \mathcal{O}\left(\ell^4\right). \tag{15}$$

Taking the second spatial derivative of Eq. (15) and multiplying with $\ell^2\rho_m/6$ yields

$$\frac{\rho_m}{6}\ell^2\ddot{u}'' = E\frac{\ell^2}{6}\frac{\rho_m}{\rho}u'''' + \frac{1}{72}\frac{\rho_m(\rho - \rho_m)}{\rho}\ell^4\ddot{u}'''' + \mathcal{O}\left(\ell^6\right) \tag{16}$$

which, when substituted back into Eq. (14), yields the following final equation of motion

$$\rho\left(\ddot{u} - \frac{\ell^2}{12}\ddot{u}'' + \left(\frac{1}{240} + \frac{1}{72}\frac{\rho_m(\rho - 2\rho_m)}{\rho^2}\right)\ell^4\ddot{u}''''\right) = E\left(u'' - \frac{\ell^2}{6}\frac{\rho_m}{\rho}u''''\right). \tag{17}$$

Comparing Eqs. (1) and (17) leads to a clear, one-to-one identification of the α, β, γ constants of the proposed three-length-scale gradient elasticity formulation

$$\alpha = \frac{1}{12}; \quad \beta = \frac{1}{240} + \frac{1}{72}\frac{\rho_m(\rho - 2\rho_m)}{\rho^2}; \quad \gamma = \frac{1}{6}\frac{\rho_{m1}}{\rho}. \tag{18}$$

Generally speaking, α may be higher or lower than γ depending on the value of the ρ_m/ρ ratio. The case $\alpha > \gamma$ is representative, for example, of fresh concrete and mortars, which corresponds to $\rho_m/\rho < 1/2$ (i.e. relatively less distributed mass and more lumped mass). On the contrary, the case $\alpha < \gamma$ has been observed in hardened concrete, which corresponds to $\rho_m/\rho > 1/2$ (i.e. relatively more distributed mass and less lumped mass).

We emphasize that we do not claim the above derivation to be the only motivation of the suggested model with strain gradients and multiple inertia gradients. What we have used is the link between the notion of lumped masses at different scales of observation and the combination of lumped mass and distributed mass at a single scale of observation. Since the distributed mass is represented by a non-diagonal mass matrix in the discrete model, continualization straightforwardly leads to inertia gradients. Obviously, other motivations may equally be possible, for example introducing series expansions of the energy functionals and applying the Hamilton's principle to obtain the equations of motion of the higher order continuum model, see Metrikine and Askes (2002, 2006) and Polyzos and Fotiadis (2012) or the next subsection.

3.2. Derivation of the proposed gradient theory through Hamilton's principle

Next, by way of complementing the continualization approach presented above, we will summarize a more formal approach to motivating the three length scale model. The kinetic and potential energy density of the three-length-scale gradient model of Eq. (5) adopt the following formats, respectively

$$\mathcal{U}^{\text{kin}} = \frac{1}{2}\rho\left[(\dot{u})^2 + \alpha\ell^2\left(\dot{u}'\right)^2 + \beta\ell^4\left(\dot{u}''\right)^2\right],$$
$$\mathcal{U}^{\text{pot}} = \frac{1}{2}E\left[\left(u'\right)^2 + \gamma\ell^2\left(u''\right)^2\right]. \tag{19}$$

Please cite this article as: D. De Domenico et al., Gradient elasticity and dispersive wave propagation: Model motivation and length scale identification procedures in concrete and composite laminates, International Journal of Solids and Structures (2018), https://doi.org/10.1016/j.ijsolstr.2018.09.007

The above energy densities form the Lagrangian density $\mathcal{L} = \mathcal{U}^{\text{kin}} - \mathcal{U}^{\text{pot}}$. The dependence of $\mathcal{L}$ upon the higher-order space derivatives of the displacement and of the velocity field is responsible for the gradient contributions in the equations of motion. For $\alpha = \beta = \gamma = 0$ the classical formats of the kinetic and potential energy density of a classical continuum are obtained. The Lagrangian function is obtained by integrating in space and time

$$L = \int_0^T \int_0^L \mathcal{L}\, \mathrm{d}x\mathrm{d}t. \tag{20}$$

Hamilton's stationary principle applied to perturbed displacement fields in (20) leads to

$$\begin{aligned} \delta L &= 0 \\ &\Rightarrow \int_0^T \int_0^L \left(\frac{\partial \mathcal{L}}{\partial \dot{u}} \delta \dot{u} + \frac{\partial \mathcal{L}}{\partial \dot{u}'} \delta \dot{u}' + \frac{\partial \mathcal{L}}{\partial \dot{u}''} \delta \dot{u}'' + \frac{\partial \mathcal{L}}{\partial u'} \delta u' + \frac{\partial \mathcal{L}}{\partial u''} \delta u'' \right) \\ \mathrm{d}x\mathrm{d}t &= 0 \end{aligned} \tag{21}$$

which, upon performing integration by parts in x and t to translate all variations to δu, yields

$$\begin{aligned} &\int_0^T \left\{ \int_0^L \left[-\frac{\partial}{\partial t}\left(\frac{\partial \mathcal{L}}{\partial \dot{u}}\right) + \frac{\partial^2}{\partial x \partial t}\left(\frac{\partial \mathcal{L}}{\partial \dot{u}'}\right) - \frac{\partial^3}{\partial t \partial x^2}\left(\frac{\partial \mathcal{L}}{\partial \dot{u}''}\right) \right.\right. \\ &\left.\left. - \frac{\partial}{\partial x}\left(\frac{\partial \mathcal{L}}{\partial u'}\right) + \frac{\partial^2}{\partial x^2}\left(\frac{\partial \mathcal{L}}{\partial u''}\right) \right] \delta u \, \mathrm{d}x \right\} \mathrm{d}t \\ &+ \int_0^T \delta u \left[\frac{\partial \mathcal{L}}{\partial u'} - \frac{\partial}{\partial x}\left(\frac{\partial \mathcal{L}}{\partial u''}\right) - \frac{\partial}{\partial t}\left(\frac{\partial \mathcal{L}}{\partial \dot{u}'}\right) + \frac{\partial^2}{\partial x \partial t}\left(\frac{\partial \mathcal{L}}{\partial \dot{u}''}\right) \right] \Bigg|_0^L \mathrm{d}t \\ &+ \int_0^T \delta u' \left[\frac{\partial \mathcal{L}}{\partial u''} - \frac{\partial}{\partial t}\left(\frac{\partial \mathcal{L}}{\partial \dot{u}''}\right) \right] \Bigg|_0^L \mathrm{d}t = 0 \end{aligned} \tag{22}$$

where account has been taken of the fact that $\delta u(x, 0) = \delta u(x, T) = 0$ and all the space and time derivatives of δu vanish at the limits of the time interval. Substituting the Lagrangian density resulting from the energy functionals in (19) into (22) straightforwardly produces the equation of motion (5) (for the first integral in (22)) and some boundary conditions (for the other two integrals).

4. Wave dispersion: analytical vs. experimental findings

In this Section we present a few experimental dispersion curves from the literature. The effectiveness of the proposed three-length-scale gradient formulation is assessed by comparing the analytical dispersion curve with the experimental findings and micromechanical data. Length-scale identification and quantification procedures are discussed, and advantages over alternative formulation of gradient elasticity theory are presented. As a remark, in real experiments finite objects are considered, whereas boundary conditions were ignored in the above theoretical model, assuming an infinite domain – this is due to their complex meaning and not clear interpretation from a physical viewpoint (De Domenico and Askes, 2016). Therefore, it is implied here that the experimental data considered below are relevant to a central zone of the material wherein boundary effects can be reasonably neglected.

4.1. Dispersion of longitudinal waves in composite laminates with periodic microstructure

We first investigate a problem in which the internal microstructure is known *a priori*, so that the corresponding material length scales can be determined exactly. The following derivations have partly been presented in (De Domenico and Askes, 2016) and are here extended to incorporate, in addition to the exact dispersion curve, some pseudo-experimental results as clarified below.

With the aid of Fig. 2, a composite laminate modeled as a one-dimensional rod with a periodic microstructure is studied. In particular, the internal microstructure is composed of two layers alternating periodically along the rod length L. In other words, the composite laminate has piecewise homogeneous material characteristics, with layer 1 being characterized by mass density ρ_1 and Young's modulus E_1, and layer 2 being defined by ρ_2 and E_2. The composite rod is considered to be very long so that the wave propagation in its periodic layer can be studied by analyzing the behavior of its *unit cell* of length ℓ. In each unit cell, materials 1 and 2 are assigned a volume fraction a and $1-a$, respectively, with $0 \leq a \leq 1$ (the limits $a = 0$ and $a = 1$ being representative of a homogeneous medium).

The periodic microstructure lends itself to the development of homogenized models having certain *effective* material properties, which approximate the behavior of the original heterogeneous medium with the main difference that the local fluctuations arising from the heterogeneities do not appear explicitly in the equation of motion. The underlying assumption is that the microscopic size ℓ of heterogeneities is significantly smaller than the macroscopic length L, at the limit $\varepsilon = \ell/L \to 0$ where ε denotes the rate of heterogeneities of the composite laminate. The homogenized equation of motion in the limit case as $\varepsilon = 0$ reads

$$\bar{\rho}\ddot{u} = \bar{E}u'' \tag{23}$$

where $\bar{\rho}$ and $\bar{E}$ are the effective mass density and the effective Young's modulus that are related to the component properties through the following relations (Andrianov et al., 2008; Chen and Fish, 2001)

$$\begin{aligned} \bar{\rho} &= a\rho_1 + (1-a)\rho_2 \\ \bar{E} &= \tfrac{E_1 E_2}{(1-a)E_1 + aE_2}. \end{aligned} \tag{24}$$

In order to account for local variations of the displacements on the scale of heterogeneities, *higher-order asymptotic homogenization* schemes with multiple length scales and time scales should be adopted (Bennett et al., 2007; Andrianov et al., 2008, 2011a,b; Chen and Fish, 2001; Fish and Chen, 2002). In Fish and Chen (2001) an asymptotic expansion including terms up to $\mathcal{O}(\epsilon^4)$ was developed according to[1]

$$\bar{\rho}\ddot{u} = \bar{E}\left(u'' + \frac{1}{12}\theta^2 \ell^2 u'''' + \frac{1}{360}\theta^2 \psi^2 \ell^4 u'''''' \right) + \mathcal{O}(\epsilon^6) \tag{25}$$

where

$$\theta = \frac{a(1-a)(E_1\rho_1 - E_2\rho_2)}{\bar{\rho}\,((1-a)E_1 + aE_2)}. \tag{26}$$

and

$$\begin{aligned} \psi = &\frac{1}{\bar{\rho}((1-a)E_1 + aE_2)} \\ &\{a^2E_2^2[2a^2\rho_1^2 - (1-a)^2\rho_2^2 + 6a(1-a)\rho_1\rho_2] \\ &+ 2a(1-a)E_1E_2[3a^2\rho_1^2 + 3(1-a)^2\rho_2^2 \\ &+ 11a(1-a)\rho_1\rho_2] - (1-a)^2E_1^2[a^2\rho_1^2 - 2(1-a)^2\rho_2^2 \\ &- 6a(1-a)\rho_1\rho_2]\}^{1/2}. \end{aligned} \tag{27}$$

After some algebra and performing some mathematical manipulations as described in De Domenico and Askes (2016), Eq. (25) may be rewritten in the following equivalent form

$$\begin{aligned} &\bar{\rho}\left(\ddot{u} - \frac{1}{12}(\theta^2+1)\ell^2\ddot{u}'' + \frac{1}{720}\theta^2\left(5(\theta^2+1) - 2\psi^2\right)\ell^4\ddot{u}'''' \right) \\ &= \bar{E}\left(u'' - \frac{1}{12}\ell^2 u'''' \right) + \mathcal{O}(\epsilon^6). \end{aligned} \tag{28}$$

[1] Unlike our earlier paper (De Domenico and Askes, 2016), account has now been taken of the misprint in the sign of the last term of Eq. (21) that was present in the original paper by (Fish and Chen, 2001), as noted in (Andrianov et al., 2011a).

Please cite this article as: D. De Domenico et al., Gradient elasticity and dispersive wave propagation: Model motivation and length scale identification procedures in concrete and composite laminates, International Journal of Solids and Structures (2018), https://doi.org/10.1016/j.ijsolstr.2018.09.007

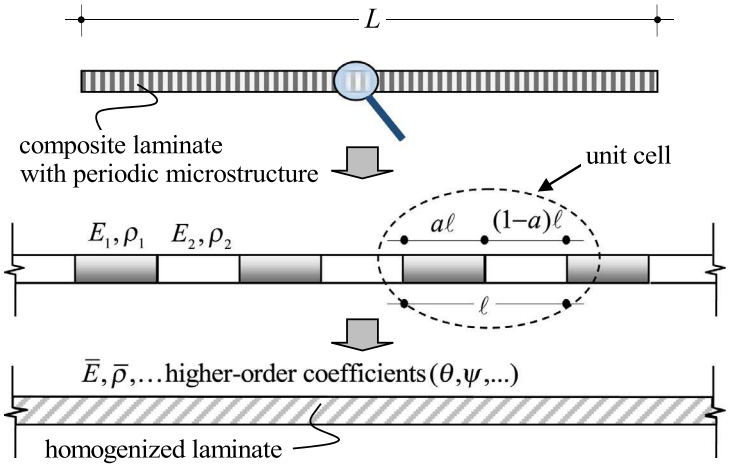

Fig. 2. Two-component composite laminate with periodically heterogeneous microstructure.

This means that the $\mathcal{O}(\epsilon^4)$ asymptotic expansion of the equations of motion of the periodic laminate shown in Fig. 2 leads to a higher-order homogenized medium described by a three-length-scale gradient elasticity formulation with one micro-stiffness and two micro-inertia terms, as that proposed in this paper. By comparing Eqs. (28) and (6), a one-to-one correspondence of the three length scale material parameters is attained as follows

$$\alpha = \frac{1}{12}(\theta^2+1), \quad \beta = \frac{1}{720}\theta^2\left(5(\theta^2+1)-2\psi^2\right), \quad \gamma = \frac{1}{12}. \tag{29}$$

Considering also that ℓ is set equal to the size of the unit cell, all the constitutive parameters of the proposed three-length-scale gradient elasticity formulation are *exactly* identified from the microstructural mechanical and physical properties of the periodic composite laminate.

Next, and in line with the goal of the present paper, we want to verify the validity of the gradient elasticity formulation reported in (28) against benchmark results. We here consider the phase velocity dispersion curve obtained from the exact solution and that arising from a "numerical simulation" of experiments (*pseudo-experimental results*). In particular, the exact dispersion curve of the periodic laminate can be obtained by applying the Floquet theorem to the periodic equations of motion (Bedford and Drumheller, 1994) and by imposing continuity of displacements and stresses at the interfaces and periodicity of the problem, which results in the following trigonometric dispersion equation (Ruzzene and Baz, 2000; Andrianov et al., 2008)

$$\cos(\bar{k}\ell) = \cos\left((\Omega(\omega))\cos\left((\Omega(\omega)\tau\right) - \frac{\xi^2+1}{2\xi}\sin\left((\Omega(\omega))\sin\left((\Omega(\omega)\tau\right)\right. \tag{30}$$

where $\bar{k}$ is the effective wave number that quantifies the nature of the wave propagation along the rod, $\Omega(\omega)=\omega L_1/c_1$ and $\tau = L_2c_1/L_1c_2$ are two material parameters depending on the two phase velocities in the two constituent materials c_1,c_2 and the lengths of the two materials within the unit cell $L_1 = a\ell$ and $L_2 = (1-a)\ell$, while $\xi = \sqrt{E_1\rho_1}/\sqrt{E_2\rho_2}$ represents the relative impedance of the composite.

On the other hand, some pseudo-experimental results are considered in addition to the exact dispersion curve presented above. These physically-based results are simulated *numerically* by means of the spectral analysis of surface waves (SASW) (Kim and Park, 2002) in conjunction with the phase spectrum approach (Sachse and Pao, 1978). This technique, mainly used in geotechnical engineering to assess in situ properties of the soil layers, has already been proposed in (Carta et al., 2012) from a numerical point of view and in (Donà et al., 2015) from an experimental point of view to identify length scale parameters of gradient elasticity theory from wave propagation. With the aid of the schematic configuration depicted in Fig. 3, the SASW technique consists of applying an impulsive load to one end of the periodically heterogeneous rod, in order to generate the propagation of an infinite series of sinusoidal waves with different frequency. The acceleration response to such impulse source is recorded at two distinct locations along the rod, namely at receiver 1 and 2. The two signals $y_1(t)$ and $y_2(t)$ from the time domain are converted into the frequency domain via the fast Fourier transform (FFT). The phases of the two signals $\varphi_1(\omega)$ and $\varphi_2(\omega)$ are then unwrapped in order to obtain two continuous functions $\varphi_{u1}(\omega)$ and $\varphi_{u2}(\omega)$, respectively. The phase velocity as a function of the frequency $c(\omega)$ is evaluated as the ratio between the product of the wave angular frequency ω times the distance between the two receivers d_2 and the shift between the two unwrapped phases, i.e.,

$$c(\omega) = \frac{\omega\, d_2}{\phi_{u1}(\omega) - \phi_{u2}(\omega)}. \tag{31}$$

Finally, the dispersion curve is plotted in terms of phase velocity against the values of the wave number for each angular frequency ω considered in the FFT analysis, the latter being computed from (31) as $k(\omega)=\omega/c(\omega)$.

The above described procedure has been applied to the periodic laminate shown in Fig. 2. The acceleration time-domain response for the application of the phase spectrum approach has been computed numerically via a finite element discretization of the heterogeneous rod with 1D-bar elements (De Domenico and Askes, 2016). The bar length is assumed as $L=100$ m, and a cross-sectional area $A=1$ m^2 for simplicity. The bar is fixed at the right hand side, and subject to a force at its left hand side $F=F_0\delta(t)$, with $\delta(t)$ the Dirac's delta and $F_0=1$N the unit-pulse applied at $t=0$. A unit cell size $\ell=0.1$ m is assumed, along with a volume fraction $a=1/2$, which means that material 1 and material 2 occupy the same volume within each unit cell. Unitary macroscopic (effective) material properties are considered, i.e. $\bar{\rho}=1\,\mathrm{kg/m^3}$ and $\bar{E}=1\,\mathrm{N/m^2}$. For given properties E_1,ρ_1 of material 1, the corresponding ones for material 2, namely E_2,ρ_2 are obtained by means of Eq. (24). Two periodic laminates with different wave dispersion characteristics are here investigated: i) the limit case of a composite laminate with *strong* contrast between the two materials by considering material 1 as a stiff, dense material, with $E_1=10^6\mathrm{N/m^2}$ and $\rho_1=1.9999\mathrm{kg/m^3}$, associated to a contrast of impedance between the two materials $\theta=0.99995$ computed from Eq. (26); ii) a heterogeneous laminate with *weak* impedance mismatch,

Please cite this article as: D. De Domenico et al., Gradient elasticity and dispersive wave propagation: Model motivation and length scale identification procedures in concrete and composite laminates, International Journal of Solids and Structures (2018), https://doi.org/10.1016/j.ijsolstr.2018.09.007

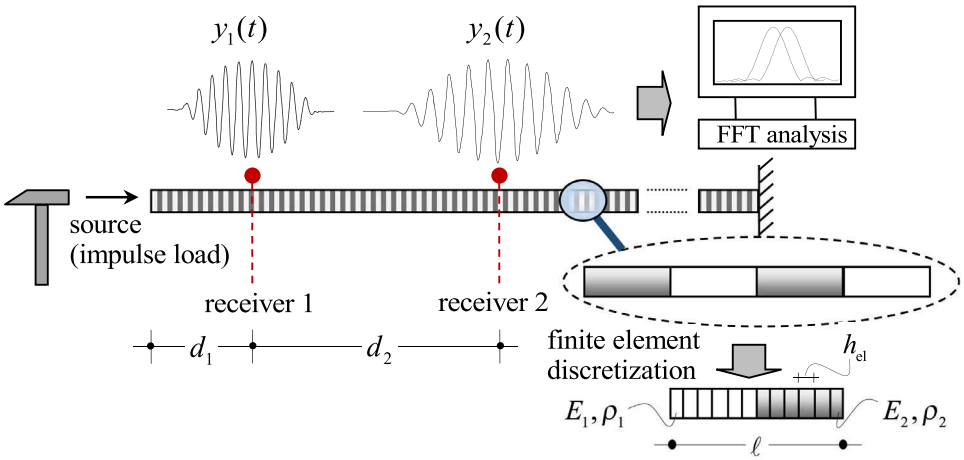

Fig. 3. Schematic configuration for determination of wave dispersion via the SASW in conjunction with the phase spectrum approach – the experimental set up is simulated numerically.

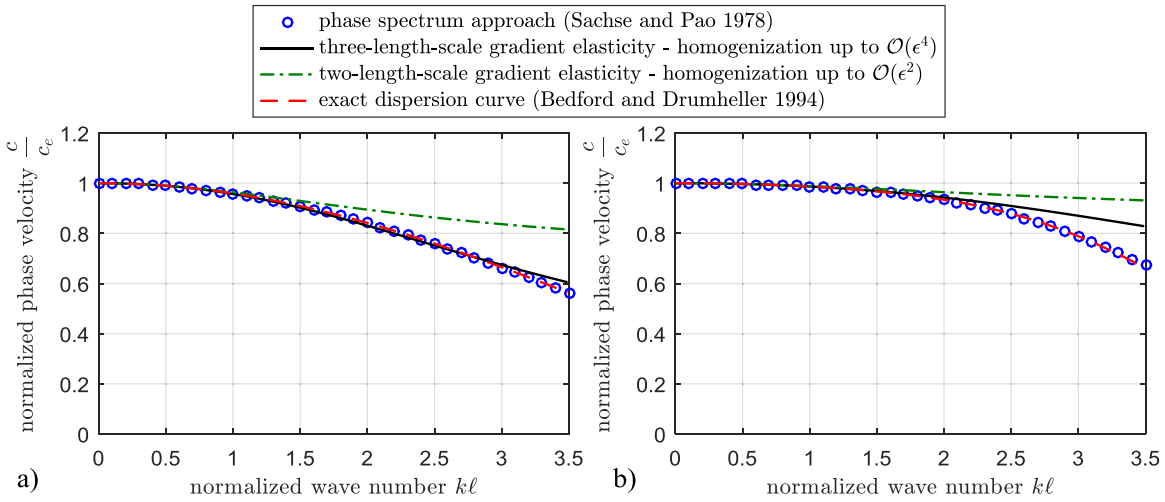

Fig. 4. Dispersion curves of periodically heterogeneous composite laminate shown in Fig. 2 with strong contrast of impedance (a) and weak contrast of impedance (b) between the two materials.

having $E_1 = 10\text{N/m}^2$ and $\rho_1 = 1.2\text{kg/m}^3$, associated with $\theta = 0.55$. In order to explicitly model the variation of the material properties within each unit cell of the laminate, the element size h_{el} is assumed as $\ell/12$. Considering that $\ell = 0.1$ m and $L = 100$ m, a mesh of 12,000 linear finite elements is employed, with periodically alternating groups of 6 elements having material properties E_1,ρ_1 and E_2,ρ_2 as shown in Fig. 3. Time integration is performed with the Newmark constant average acceleration scheme, with a time step $\Delta t = h_{\text{el}}$ in accordance with the guidelines indicated in (De Domenico and Askes, 2017). It has been found that the position of the two receivers does not affect the wave dispersion results appreciably (Carta et al., 2012), therefore we have assumed $d_1 = 1$ m and $d_2 = 1$ m for simplicity.

Exact dispersion curve, phase spectrum approach and gradient elasticity results (with both two and three length scales) are all reported in Fig. 4 and compared to each other. The exact solution in terms of phase velocity is derived by solving the trigonometric Eq. (30) numerically for ω, and then obtaining $c = \omega/\bar{k}$. The two length scale gradient elasticity formulation is obtained as a special case of the three-length-scale case by eliminating the ℓ^4 term in (28). Such solution corresponds to an asymptotic homogenization that is accurate up to $\mathcal{O}(\epsilon^2)$, whereas the three-length-scale formulation is a $\mathcal{O}(\epsilon^4)$ homogenized model (De Domenico and Askes, 2016).

By inspection of Fig. 4 it is seen that, as expected, the laminate with strong impedance mismatch between the two materials, case i), is more dispersive than the laminate with weak contrast, case ii). In both cases it is observed that the exact dispersion curve is almost coincident with the one provided by the phase spectrum approach, which confirms that the numerically simulated pseudo-experimental results are fully consistent with the material properties of the laminate and the chosen finite element mesh is appropriate. This result is valuable: indeed, it is expected that a reference (numerical) solution could be identified for other more complicated microstructural arrangements of the laminate, for which an exact solution is not available in the literature, by simulating the phase spectrum experiments as done in this simple example. The analytical dispersion curves provided by the three-length-scale gradient elasticity model, Eq. (6) equipped with the constants identified in (29), gives a very precise description of the exact dispersion curve of the heterogeneous medium for all the depicted range of normalized wave numbers in the laminate with strong impedance mismatch, and up to approximately $k\ell \approx 2.5$ for the laminate with weak contrast. It is worth noting that the correction in the sign of the last term in Eq. (25) has led to certain improvements as compared to the results shown in an earlier paper of the authors (De Domenico and Askes, 2016). In both cases, the introduction of the β term leads to significant improvements as

Please cite this article as: D. De Domenico et al., Gradient elasticity and dispersive wave propagation: Model motivation and length scale identification procedures in concrete and composite laminates, International Journal of Solids and Structures (2018), https://doi.org/10.1016/j.ijsolstr.2018.09.007

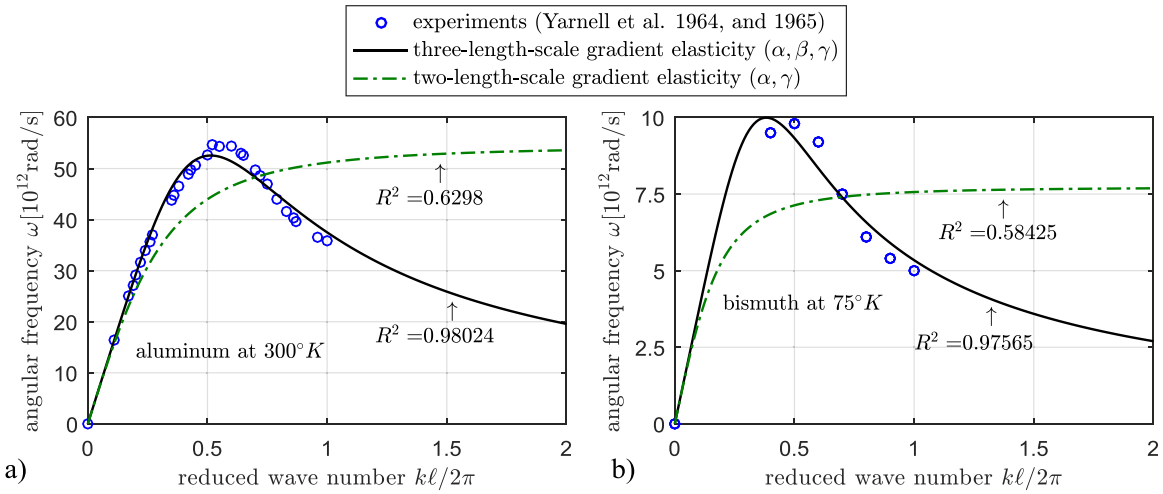

Fig. 5. Analytical versus experimental dispersion curves for phonons propagating in the longitudinal direction for aluminum (a) and bismuth (b) (experimental data after Yarnell et al., 1964b, 1965).

compared to the two-length-scale model without β. More importantly, the third length scale plays a crucial role in fitting the exact dispersion curve while not requiring additional computational cost: the same finite element implementation can be used for both the three-length-scale and two-length-scale gradient elasticity model (see (De Domenico and Askes, 2016) for full details).

4.2. Phonon dispersion in aluminum and bismuth

Neutron scattering experiments were conducted by Yarnell and co-workers in the mid-sixties to investigate the dispersion characteristics of waves propagating in nano-structured materials. In particular, experimental dispersion curve for phonons propagating in the longitudinal crystallographic direction in an aluminum crystal at 300°K and in bismuth at both room temperature and at 75°K were reported in two research works (Yarnell et al., 1964b, 1965) in the shape of angular frequency versus normalized wave number curve. Relevant results are shown in Fig. 5 (for bismuth, only the results at 75°K are reported; at room temperature the observed frequencies were about 1.5% lower than the displayed case).

Based on the experimental results, the analytical dispersion curves from gradient elasticity theory have been constructed, and the main length-scale parameters entering Eq. (6) have been found as a result of a non-linear least square minimization procedure. Two theoretical dispersion curves are shown and compared in Fig. 5, namely the three-length-scale gradient elasticity formulation with α, β, γ terms, and the two-length-scale formulation with only α, γ terms, i.e., by excluding the second micro-inertia term proportional to β. The values of the coefficient of determination R^2 are also displayed in the same figures, showing very good agreement for the three-length-scale formulation, and a rather poor performance of the two-length-scale model. The α, β, γ coefficients identified from the minimization procedure are $\alpha = 0.01233$, $\beta = 0.009199$ and $\gamma \approx 0$ for aluminum, and $\alpha \approx 0$, $\beta = 0.03015$ and $\gamma \approx 0$ for bismuth, which highlights the importance of including the second micro-inertia term. Without this term, the change of the curvature (inflexion point) that is experimentally observed in the medium wave number regime cannot be captured. It can demonstrated, see e.g. (De Domenico and Askes, 2016), that the occurrence of such an inflexion in the dispersion curve results from the circumstance $\beta > \alpha\gamma$ in the corresponding dispersion Eq. (6), which is a condition fully met by the aforementioned identified coefficients. The fact that α is small for bismuth is a particularity of this set of experiments, while the circumstance $\gamma \approx 0$ found for the two analyzed cases would imply that the dispersion curve has a zero asymptote for infinitely large wave numbers. However, it is clear that experimental evidence for the very large wave numbers is lacking, which suggests that the result $\gamma \approx 0$ may be a mathematical peculiarity of this particular set of experimental data.

4.3. Dispersion of longitudinal waves in fresh and hardened concrete specimens

Concrete is a highly non-homogeneous (particulate composite) material containing random inhomogeneities over a wide range of length scales (cement, sand, fine and coarse aggregates, air bubbles suspended in water, etc.), which is reflected in its complicated mechanical behavior (De Domenico, 2015; De Domenico et al., 2014; Pisano et al., 2014, 2015). Closely related to the complex and randomly organized microstructure of concrete, wave dispersion is induced by multiple wave scattering phenomena, with a stress wave undergoing both dispersion and attenuation when propagating through such a non-homogeneous material (Kim et al., 1991; Jacobs and Owino, 2000). In the relevant literature, measurements concerning ultrasonic wave propagation on concrete specimens were mainly related to determination of the actual water/cement (w/c) ratio (Popovics and Popovics, 1998), as well as to estimate other material properties such as strength, porosity and damage of concrete (Malhotra and Carino, 1991). For instance, concrete specimens with lower w/c ratio were found to exhibit higher wave velocity as well as higher amplitude measured through transmission (Ye et al., 2003), and the concrete pulse velocity was found to be frequency-dependent especially over the range of 24–120 kHz (Popovics et al., 1990).

A well-documented experimental campaign concerning ultrasonic wave propagation on fresh and hardened concrete as well as on mortar specimens was conducted at the University of Patras (Aggelis et al., 2005; Philippidis and Aggelis, 2005). This study, here referred to for the experimental findings, was aimed at assessing the quality of concrete at different stages after mixing via ultrasonic non-destructive testing techniques. The dispersive features observed in ultrasonic wave propagation were ascribed to the underlying internal microstructure of concrete. In particular, two material properties were explored, namely the sand content and the w/c ratio.

In Figs. 6 and 7 the experimental results in terms of phase velocity curves of fresh concrete specimens (Aggelis et al., 2005) are displayed. These results were obtained through a waveform

Please cite this article as: D. De Domenico et al., Gradient elasticity and dispersive wave propagation: Model motivation and length scale identification procedures in concrete and composite laminates, International Journal of Solids and Structures (2018), https://doi.org/10.1016/j.ijsolstr.2018.09.007

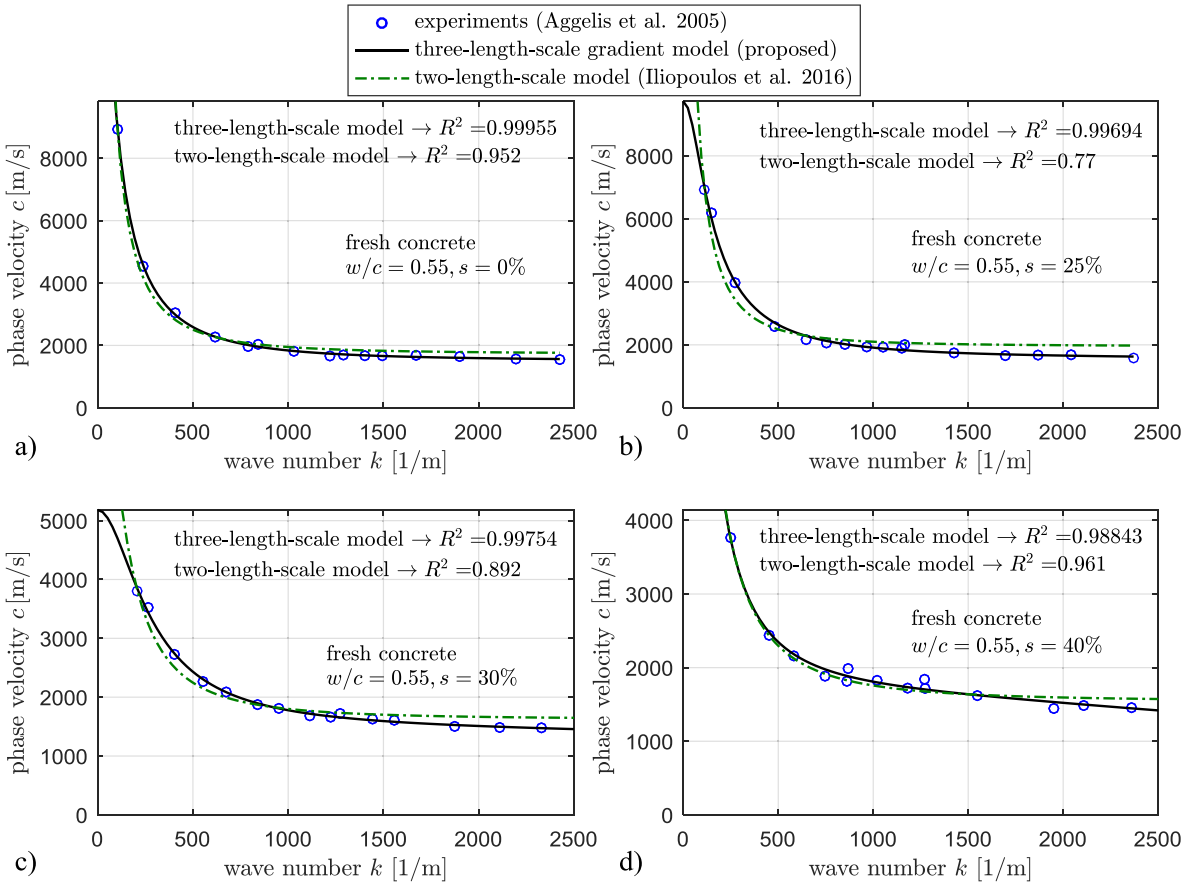

Fig. 6. Analytical versus experimental dispersion curves of fresh concrete specimens with w/c ratio equal to 0.55 and different sand contents: a) $s = 0\%$; b) $s = 25\%$; c) $s = 30\%$; d) $s = 40\%$ (experimental data after Aggelis et al., 2005).

generator and two broadband piezoelectric transducers, which were installed on two opposite faces of a special Plexiglas U-shaped mold in which the fresh cementitious material was poured. A set of tone-burst signals were introduced into the specimens, with central frequencies ranging from 20 kHz up to about 1 MHz, and the signals at the two sensors located at a given separation distance were monitored. The phase velocity was determined for each frequency as the ratio of the distance traveled over the delay observed in the two waveforms (Kinra et al., 1980). Although the source experimental plots were in the form of phase velocity c versus frequency f curves (Aggelis et al., 2005), for consistency with the remainder of the paper the experimental results are here presented as phase velocity versus wave number curves by recalling the relation $k = 2\pi f/c$. In this way, the length scale parameters entering the gradient elasticity formulation of Eq. (6) can be found by a data fitting of the experimental pairs $c - k$ with a non-linear least square minimization procedure.

The corresponding analytical dispersion curves provided by the gradient elasticity theory are reported against the experimental findings. The specimens shown in Fig. 6 share the same w/c ratio equal to 0.55, while the sand content varies from zero (limit case of the cement paste) to 25%, 30% and 40%. Conversely, fresh concrete specimens reported in Fig. 7 share the same sand content equal to $s = 30\%$ while the w/c ratio assumes the values 0.46, 0.475, 0.525, 0.55. The size of sand particles in both cases ranged from 1 mm to 4 mm.

By inspection of the experimental points, significant dispersion is observed as the phase velocity values drop from several thousand m/s to approximately the sound velocity in water (1500 m/s) for the large wave numbers. It is worth noting that in some cases extremely high values of phase velocity would be extrapolated in the low wave number regime, see e.g. Fig. 6a, b and d. This behavior cannot be explained by classical approaches, but rather it may be ascribed to the interaction between micro-structural effects (Iliopoulos et al., 2016) and to the resonance behaviors of air bubbles within fresh concrete that is still in a liquid form. From Fig. 6, it is noted that an increase of sand content from 0% to 40% produces a decrease in the phase velocity in the low wave number range, whereas in the medium-to-high wave number range the phase velocity is found to be not significantly affected by the sand content. This implies that the stiffer the mortar, due to an increase of the sand content, the less the dispersion experimentally obtained. On the contrary, from Fig. 7 it is observed that an increase of the w/c ratio yields a more dispersive wave propagation, as the phase velocities in the low-frequency regime increase accordingly. Therefore, the stronger dispersive behavior is observed for the less stiff specimens, with low sand content and high water content.

In Iliopoulos et al. (2016) the two-length-scale gradient elasticity model with one micro-stiffness term and one micro-inertia term ($\alpha\ell^2$ and $\gamma\ell^2$ terms of the present notation, which in the quoted paper were termed as h^2 and g^2) was employed to describe the dispersive wave propagation analytically, and the corresponding length scale parameters were detected as a result of a least square fitting technique against the experimental data. In Tables 1 and 2 the microstructural parameters h and g as well as the R^2 values directly taken from the study by Iliopoulos et al. (2016) are listed. As an extension of this model, we here repeat the curve fitting procedure by using the three-length-scale gradient elasticity formulation as per Eq. (6). The corresponding R^2 values are

Please cite this article as: D. De Domenico et al., Gradient elasticity and dispersive wave propagation: Model motivation and length scale identification procedures in concrete and composite laminates, International Journal of Solids and Structures (2018), https://doi.org/10.1016/j.ijsolstr.2018.09.007

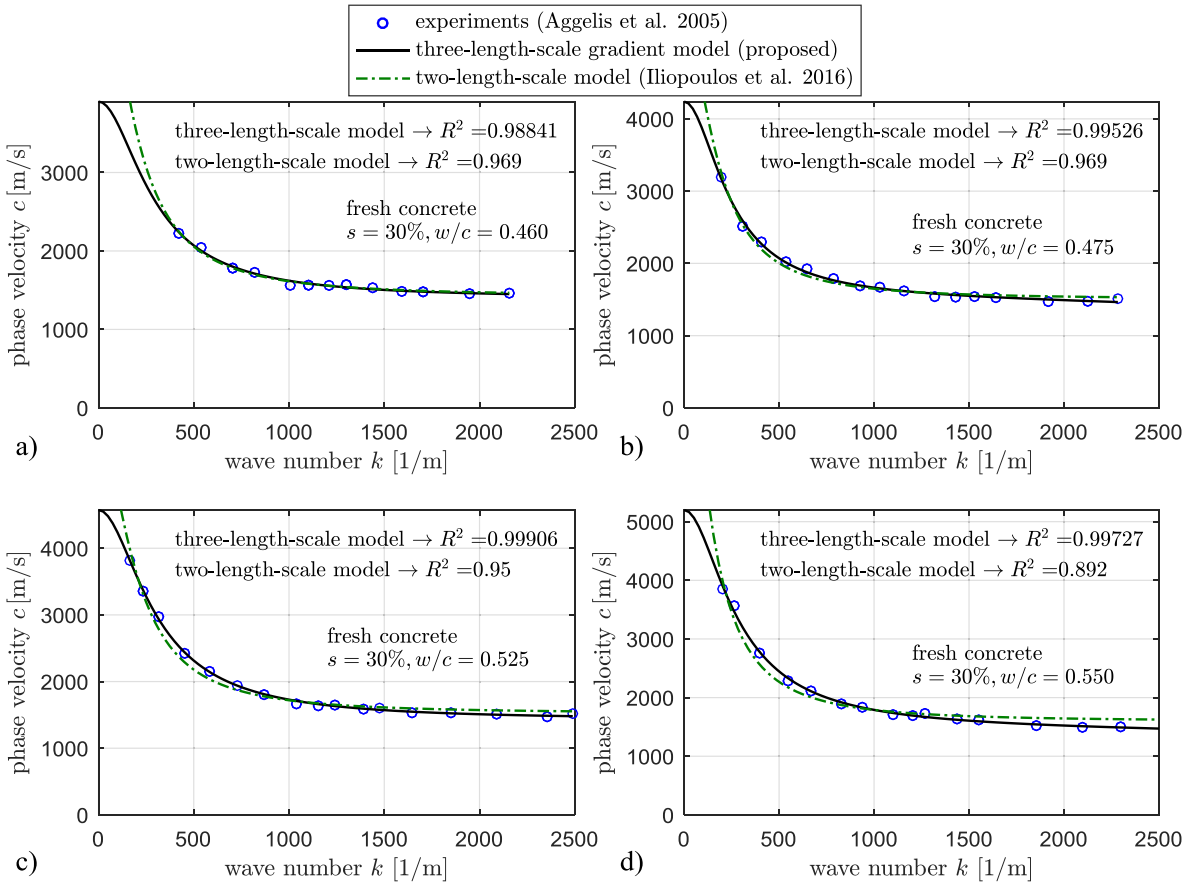

Fig. 7. Analytical versus experimental dispersion curves of fresh concrete specimens with $s = 30\%$ and different w/c ratios: a) $w/c = 0.460$; b) $w/c = 0.475$; c) $w/c = 0.525$; d) $w/c = 0.550$ (experimental data after Aggelis et al., 2005).

Table 1
Length scale identification for fresh concrete specimens with water/cement ratio equal to $w/c = 0.55$ and different sand contents (experimental data after Aggelis et al., 2005).

	three-length-scale gradient elasticity model (proposed)					two-length-scale gradient model (Ilioupoulos et al. 2016)		
sand content	c_e [m/s^2]	$h = \sqrt{\alpha\ell^2}$ [m]	$\tilde{h} = \sqrt[4]{\beta\ell^4}$ [m]	$g = \sqrt{\gamma\ell^2}$	R^2	h [m]	g [m]	R^2
0%	17,820	0.0167	0.0106	0.0014	0.99955	0.3243	0.0019	0.952
25%	9728	0.0089	0.0181	0.0015	0.99694	0.0300	0.0025	0.770
30%	5182	0.0047	0.0189	0.0013	0.99754	0.0103	0.0020	0.892
40%	70,240	0.0839	0.0833	0.0020	0.98843	0.4896	0.0018	0.961

Table 2
Length scale identification for fresh concrete specimens with sand content $s = 30\%$ and different water/cement ratios (experimental data after Aggelis et al., 2005).

	three-length-scale gradient elasticity model (proposed)					two-length-scale gradient model (Ilioupoulos et al. 2016)		
w/c ratio	c_e [m/s^2]	$h = \sqrt{\alpha\ell^2}$ [m]	$\tilde{h} = \sqrt[4]{\beta\ell^4}$ [m]	$g = \sqrt{\gamma\ell^2}$	R^2	h [m]	g [m]	R^2
0.460	3904	0.0043	0.0012	0.0016	0.98841	0.0076	0.0018	0.969
0.475	4240	0.0052	0.0216	0.0018	0.99526	0.0074	0.0021	0.969
0.525	4574	0.0043	0.0009	0.0013	0.99906	0.0068	0.0018	0.950
0.550	5199	0.0047	0.0191	0.0013	0.99727	0.0102	0.0019	0.892

appreciably higher than the ones reported in Iliopoulos et al. (2016) because of the added fourth-order term, and the agreement with the experimental data is excellent for all the analyzed concrete specimens, cf. again Figs. 6 and 7. Interestingly, from Tables 1 and 2 it is noted that the length-scale parameters associated with the strain gradient term, $g = \sqrt{\gamma\ell^2}$, is roughly similar in the two gradient elasticity models equipped with two- and three-length-scale parameters, respectively. In particular, this length scale has dimensions ranging from 1.3 mm to 2.0 mm for the three-length-scale model and from 1.8 mm to 2.5 mm for the two-length-scale model, which in both cases resembles the average size of the sand particles adopted in the analyzed fresh concrete specimens. Therefore, a consistent relationship between the length scale parameter and the characteristic size of the material microstructure exists, which was also observed in (Iliopoulos et al., 2016). On the contrary, the micro-inertia term $h = \sqrt{\alpha\ell^2}$ in the two gradient elasticity models equipped with two- and three-length-scale parameters are rather different, which is also quite

Please cite this article as: D. De Domenico et al., Gradient elasticity and dispersive wave propagation: Model motivation and length scale identification procedures in concrete and composite laminates, International Journal of Solids and Structures (2018), https://doi.org/10.1016/j.ijsolstr.2018.09.007

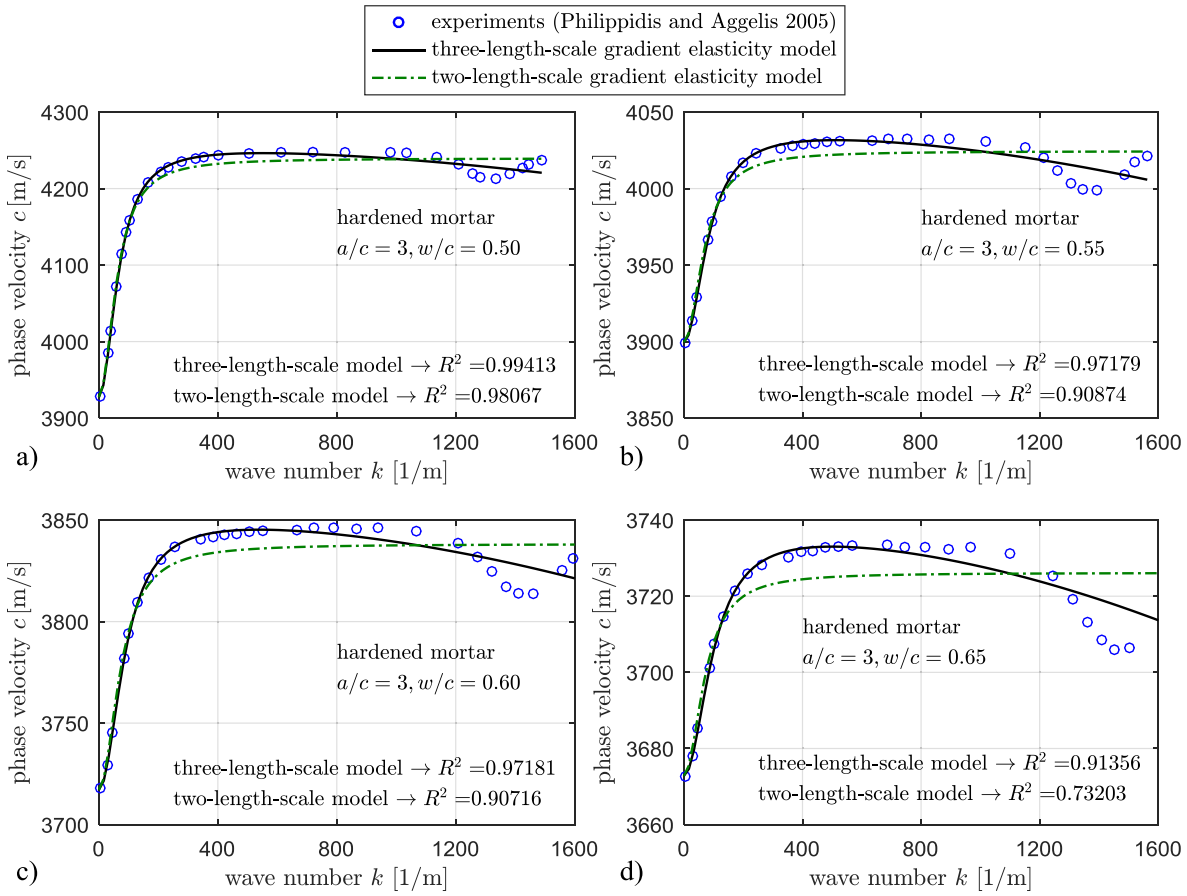

Fig. 8. Analytical versus experimental dispersion curves of hardened mortar specimens with $a/c = 0.3$ and different w/c ratios: a) $w/c = 0.50$; b) $w/c = 0.55$; c) $w/c = 0.60$; d) $w/c = 0.65$ (experimental data after Philippidis and Aggelis, 2005).

reasonable as the three-length-scale model describes the micro-inertia effects via an additional micro-inertia term $\bar{h} = \sqrt[4]{\beta \ell^4}$ in comparison with the two-length-scale gradient model. In all the fresh concrete specimens it is found that $h > g$, which means that $\alpha > \gamma$ in Eq. (6).

This circumstance generates a phase velocity curve that is decreasing with increasing wave numbers, i.e., the higher wave numbers travel slower than the lower wave numbers. This behavior is typical of fresh mortar and fresh concrete specimens where the inclusions, in the form of sand particles, are embedded in a liquid matrix, thus micro-inertia values are higher than micro-stiffness.

On the other hand, mortar and concrete specimens were also tested at a hardened state (Philippidis and Aggelis, 2005) and the corresponding experimental phase velocity curve was derived. The phase spectrum technique introduced in (Sachse and Pao, 1978) was employed: two ultrasonic broadband transducers, having center frequency 500 kHz and mounted directly on the specimen surface, were used, the fast Fourier transforms of the exciting and received signals were recorded and the difference of unwrapped phases for each frequency component of the Fourier spectrum was calculated, thus giving indications on the phase velocity for that frequency. Cubic specimens of 150 mm side were tested, aged between 2.5 and 4 years from casting (Philippidis and Aggelis, 2005). Mortar specimens contain cement, sand and water, with sand particles up to 4.75 mm, whereas concrete specimens contain also fine aggregates, ranging from 1.18 mm to 25 mm, and coarse aggregates, of sizes from 4.75 mm to 37.5 mm. Phase velocity curves for mortar and concrete specimens are reported in Figs. 8 and 9, respectively. Different w/c ratios are examined, while all the specimens share the same aggregate to cement ratio $a/c = 3$, resulting in volume content of aggregates of approximately 60%. It is found that both mortar and concrete specimens at hardened state exhibit an opposite dispersive behavior than the fresh cementitious specimens discussed before, as the phase velocity curve increases with increasing wave numbers, which means that the higher wave numbers travel faster than the lower wave numbers. Generally speaking, concrete specimens exhibit a more pronounced dispersive behavior than mortar ones, which is reflected by the higher increase of phase velocity in the low wave number range. This may be due to the larger size of inclusions in the form of coarse aggregates that contribute to an increased inhomogeneity of the specimen as a whole.

The analytical dispersion curves from gradient elasticity theory are reported against the experimental data. The microstructural coefficients of both the three-length-scale and the two-length-scale gradient formulation are again identified via a non-linear least square minimization procedure and reported in Tables 3 and 4 for mortar and concrete, respectively. For hardened concrete specimens, the two length-scale parameters h and g as well as the R^2 values are directly taken from the study by Iliopoulos et al. (2016). Similarly to the case of fresh concrete, for hardened concrete significant improvements are achieved by the inclusion of an additional micro-inertia term, with the R^2 values of the three-length-scale model being appreciably higher (in all cases higher than 0.99) than the ones obtained by the two-length-scale gradient formulation in Iliopoulos et al. (2016), cf. Table 4. Excellent performance is also achieved with regard to mortar specimens, cf. Table 3. Due to the shape of the phase velocity curve that increases with

Please cite this article as: D. De Domenico et al., Gradient elasticity and dispersive wave propagation: Model motivation and length scale identification procedures in concrete and composite laminates, International Journal of Solids and Structures (2018), https://doi.org/10.1016/j.ijsolstr.2018.09.007

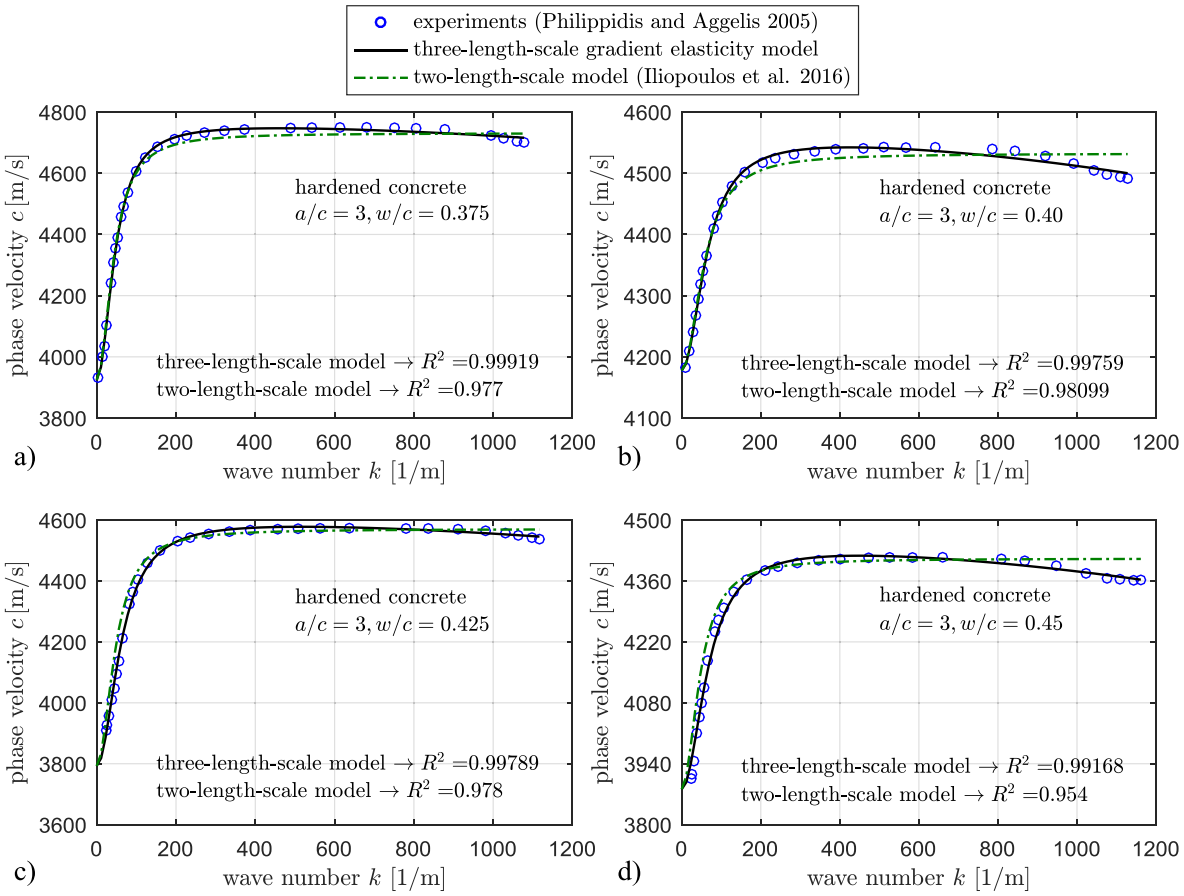

Fig. 9. Analytical versus experimental dispersion curves of hardened concrete specimens with $a/c = 0.3$ and different w/c ratios: a) $w/c = 0.375$; b) $w/c = 0.40$; c) $w/c = 0.425$; d) $w/c = 0.45$ (experimental data after Philippidis and Aggelis, 2005).

Table 3
Length scale identification for hardened mortar specimens with aggregate to cement mass ratio $a/c = 3$ and different water/cement ratios (experimental data after Philippidis and Aggelis, 2005).

	three-length-scale gradient elasticity model					two-length-scale gradient elasticity model		
w/c ratio	c_e [m/s^2]	$h = \sqrt{\alpha \ell^2}$ [m]	$\bar{h} = \sqrt[4]{\beta \ell^4}$ [m]	$g = \sqrt{\gamma \ell^2}$	R^2	h [m]	g [m]	R^2
0.500	3927	0.0146	0.0069	0.0158	0.999413	0.0159	0.0172	0.98067
0.550	3900	0.0118	0.0061	0.0122	0.97179	00,141	0.0146	0.90874
0.600	3717	0.0112	0.0060	0.0116	0.97181	0.0134	0.0138	0.90716
0.650	3673	0.0101	0.0062	0.0102	0.91356	0.0137	0.0139	0.73203

Table 4
Length scale identification for hardened concrete specimens with aggregate to cement mass ratio $a/c = 3$ and different water/cement ratios (experimental data after Philippidis and Aggelis, 2005).

	three-length-scale gradient elasticity model (proposed)					two-length-scale gradient model (Iliopoulos et al., 2016)		
w/c ratio	c_e [m/s^2]	$h = \sqrt{\alpha \ell^2}$ [m]	$\bar{h} = \sqrt[4]{\beta \ell^4}$ [m]	$g = \sqrt{\gamma \ell^2}$	R^2	h [m]	g [m]	R^2
0.375	3925	0.0203	0.0072	0.0246	0.99919	0.0219	0.0264	0.977
0.400*	4178	0.0153	0.0078	0.0167	0.99759	0.0169	0.0183	0.981
0.425	3793	0.0154	0.0080	0.0187	0.99789	0.0200	0.0247	0.978
0.450	3881	0.0144	0.0071	0.0165	0.99168	0.0205	0.0238	0.954

* This case was not discussed in the study by Iliopoulos et al. (2016). The results with the two-length-scale gradient elasticity model are derived by the authors.

increasing wave numbers, in all the hardened mortar and concrete specimens it is found that $g > h$, which means that $\gamma > \alpha$ in Eq. (6). This behavior is typical of hardened concrete where inclusions, in the form of coarse aggregates, are harder than the solid matrix and micro-stiffness attains higher values than micro-inertia.

In Tables 3 and 4 it is found that the microstructural coefficients $g = \sqrt{\gamma \ell^2}$ and $h = \sqrt{\alpha \ell^2}$ are roughly comparable in the two gradient elasticity models equipped with two- and three-length-scale parameters, respectively. In particular, the microstructural coefficient g has dimensions of a few cm, more specifically ranging from 16.5 mm to 24.6 mm for the three-length-scale model and from 18.3 mm to 26.4 mm for the two-length-scale model. These results are both consistent with the average size of aggregates used for concrete specimens (mean size 24 mm (Iliopoulos et al., 2016)).

Please cite this article as: D. De Domenico et al., Gradient elasticity and dispersive wave propagation: Model motivation and length scale identification procedures in concrete and composite laminates, International Journal of Solids and Structures (2018), https://doi.org/10.1016/j.ijsolstr.2018.09.007

Comparing these values with the previous ones for fresh concrete specimens, it is found that the length scale parameter g is a few mm in the case of fresh concrete, and a few cm in the case of hardened concrete. This order of magnitude of difference reflects the actual particle sizes in the underlying material microstructure at the two different states, as already noted in Iliopoulos et al. (2016). Moreover, by inspection of Tables 3 and 4 it can be noted that an increase of the w/c ratio leads to a monotonic decrease of the micro-stiffness g, which is physically reasonable as the macroscopic representative volume contains a higher amount of water. The results of concrete specimen with $w/c = 0.400$ slightly deviate from this trend, probably due to some experimental troubles occurred during this specific tests.

The phase velocity value c_e in the limit as $k \to 0$ (characterizing the wave propagation of non-dispersive waves in a classical elastic medium) decreases with increasing the w/c ratio. The c_e values in hardened mortar and hardened concrete approximately range from 3700 to 4000 m/s, which are physically consistent values for typical concrete properties in terms of mass density $\rho \approx 2400\,\mathrm{kg/m^3}$ and Young's modulus $E \approx 2.8 \cdot 10^{10}\mathrm{N/m}$. For such typical concrete properties the classical one-dimensional phase velocity would be $c_e = \sqrt{E/\rho} \approx 3400\,\mathrm{m/s}$. However, the actual dispersive behavior experimentally occurring in the concrete specimens is not described by the one-dimensional equation of motion (5), but rather by Eq. (1). The dispersive properties of Eq. (1) were derived in De Domenico and Askes (2017) by studying two-dimensional wave propagation. The following results were obtained in terms of compressive and shear wave velocity, respectively

$$\frac{c^2}{c_p^2} = \frac{1+\gamma\chi^2}{1+\alpha\chi^2+\beta\chi^4} \quad \text{with } c_p^2 = \frac{\lambda+2\mu}{\rho} = \frac{E}{\rho}\frac{(1-\nu)}{(1+\nu)(1-2\nu)} = c_e^2\frac{(1-\nu)}{(1+\nu)(1-2\nu)}$$
$$\frac{c^2}{c_s^2} = \frac{1+\gamma\chi^2}{1+\alpha\chi^2+\beta\chi^4} \quad \text{with } c_s^2 = \frac{\mu}{\rho} = \frac{E}{2\rho(1+\nu)} \tag{32}$$

where λ, μ are the Lamé constants, while c_p and c_s denote the long wave length limit of the compressive and shear wave velocity, respectively. The comparison between Eqs. (6) and (32) reveals that the dispersion curves for one-dimensional waves and two-dimensional compressive and shear waves have the same shape, the only difference being the factor by which they are scaled. The one-dimensional case may be retrieved from Eq. (32) for a zero value of the Poisson's ratio ν, leading to $c_p \equiv c_e = \sqrt{E/\rho}$. For $\nu > 0$ one has $c_p > c_e$; again referring to typical medium concrete properties and considering that the Poisson's ratio can be assumed as $\nu \approx 0.2 - 0.3$, the ratio c_p^2/c_e^2 in (32) is roughly equal to $(1-\nu)/(1+\nu)(1-2\nu) \approx 1.11 - 1.35$, so that $c_p \approx 1.05 - 1.16\,c_e$, which is definitely in agreement with the phase velocity values found in the experimental dispersion curves in the limit as $k \to 0$ for a classical phase velocity of approximately $c_e = \sqrt{E/\rho} \approx 3400\,\mathrm{m/s}$.

In order to establish a direct link between the length-scale parameters and the geometric and mechanical properties of the microstructure, the lattice model described in Section 3.1 can be resorted to. To this aim, the procedure described in (Iliopoulos et al., 2016) is here adapted to link the proposed three-length-scale gradient elasticity formulation to the microstructure of the hardened concrete specimens. In particular, the Young's modulus of the lattice model illustrated in Fig. 1 is expressed according to the mixture law as follows

$$E = E_a V_a + E_m V_m \tag{33}$$

where E_a and E_m denote the Young's modulus of the concrete aggregates and concrete matrix, respectively, while V_a and V_m are the corresponding volume fractions, with $V_m = 1 - V_a$. For the tested concrete specimens, these mechanical and physical quantities were experimentally evaluated and are reported in Table 5 for each w/c ratio. It is noted that the Young's modulus of the matrix E_m monotonically decreases as the w/c ratio increases, which is reasonable since the water content negatively influences the matrix stiffness. The concrete Young's modulus E calculated according to Eq. (33) is also listed in the Table.

Table 5
Physical and mechanical properties of concrete specimens (after Iliopoulos et al., 2016).

	aggregates			Matrix			concrete
w/c	E_a [GPa]	ρ_a [kg/m^3]	V_a [–]	E_m [GPa]	ρ_{mat} [kg/m^3]	V_m [–]	E [GPa]
0.375	70	2650	0.310	20.0	2100	0.690	35.5
0.400*	70	2650	0.305	18.5	2090	0.695	34.2
0.425	70	2650	0.300	17.0	2080	0.700	32.9
0.450	70	2650	0.290	14.0	2050	0.710	30.2

* This case was not discussed in Iliopoulos et al. (2016). Mechanical and physical properties are here estimated by the authors on the basis of the other results.

We also compute the total mass density of the lattice system $\rho = \rho_M + \rho_m$, with ρ_M denoting the macro-volume density and ρ_m indicating micro-volume density, cf. Fig. 1. These mass density terms are linked to the physical properties of the concrete specimens through the expressions

$$\rho_M = \rho_a\, V_a, \quad \rho_m = \rho_{mat}\, V_m \tag{34}$$

where ρ_a and ρ_{mat} denote the aggregate and matrix densities. Value of the parameters ρ_a,ρ_{mat} experimentally evaluated for each concrete specimen are listed in Table 5. The ρ_m/ρ ratio expressing the significance of the micro-to-macro density is then computed for each concrete specimen and reported in Table 6 as well. Once the ρ_m/ρ ratio is computed, the particle spacing ℓ of the nonlocal lattice model, representing the unit cell of the non-homogeneous material, can be derived from the micro-stiffness g as follows

$$g^2 = \gamma\,\ell^2 = \frac{\rho_m}{6\rho}\ell^2 \rightarrow \quad \text{determine } \ell. \tag{35}$$

To determine ℓ, the values of the length-scale material parameter g identified with the non-linear least square fitting procedure and reported in Table 4 have been assumed. The obtained lattice size ℓ for each w/c ratio is reported in Table 6. The particle size ℓ may also be used to determine the mean aggregate diameter d. On the basis of the volume fraction V_a, the mean aggregate diameter has been estimated as $d \approx \ell\sqrt[3]{V_a}$, see Iliopoulos et al. (2016), which ranges from $d = 51.0$ mm for $w/c = 0.375$ to $d = 33.1$ mm for $w/c = 0.45$ as reported in Table 6. Except for the case $w/c = 0.375$, these values are quite in line with the actual aggregate dimensions used for the hardened concrete specimens, so that the obtained d values may realistically describe the representative concrete microstructure.

Once the particle spacing ℓ is determined, the micro-inertia length scales of the nonlocal lattice model are finally calculated as

$$h^2 = \alpha\ell^2 = \frac{1}{12}\ell^2, \quad \bar{h}^4 = \beta\ell^4 = \left(\frac{1}{240} + \frac{1}{72}\frac{\rho_m(\rho - 2\rho_m)}{\rho^2}\right)\ell^4 \tag{36}$$

in line with the previously discussed Eq. (17). The resulting micro-inertia terms calculated through (36) are reported in Table 6 as well. Two main conclusions may be drawn: 1) all the calculated micro-inertia values h are lower than the corresponding micro-stiffness g, which confirms the result obtained by fitting the experimental dispersion curves; 2) such micro-inertia terms h and $\bar{h}$ derived from the nonlocal lattice model roughly resemble the values of h and $\bar{h}$ identified by curve fitting the experimental dispersion curves, cf. Table 4. This result is not trivial, as these two sets

Please cite this article as: D. De Domenico et al., Gradient elasticity and dispersive wave propagation: Model motivation and length scale identification procedures in concrete and composite laminates, International Journal of Solids and Structures (2018), https://doi.org/10.1016/j.ijsolstr.2018.09.007

Table 6
Link between nonlocal lattice parameters and concrete microstructure.

	nonlocal lattice		concrete microstructure parameters derived from lattice model			
w/c	$\frac{\rho_m}{\rho}$	ℓ [m]	d [m]	$g=\sqrt{\gamma\ell^2}$	$h=\sqrt{\alpha\ell^2}$ [m]	$\tilde{h}=\sqrt[4]{\beta\ell^4}$ [m]
0.375	0.638	0.0754	0.05105	0.0246	0.0217	0.0154
0.400	0.642	0.0510	0.03435	0.0167	0.0147	0.0102
0.425	0.647	0.0569	0.03813	0.0187	0.0164	0.0111
0.450	0.654	0.0499	0.03307	0.0165	0.0144	0.0096

of micro-inertia terms arise from two different procedures, the former focused on mathematically-based least square principles, the latter inspired by a physically-based approach via the proposed nonlocal lattice model.

5. Concluding remarks

Elastic waves propagating through non-homogeneous media exhibit dispersion if their wavelength is of the same order as the characteristic length scale of the material microstructure. In order to capture such physical phenomenon, in this paper gradient enrichments of the classical continuum equations have been employed. In the literature, a number of gradient elasticity formulations were proposed, mainly originating from the Mindlin's theory of elasticity with microstructure. In the framework of wave dispersion one of the most popular models is the one equipped with two length scale parameters, associated with one higher-order stiffness term (strain gradient) and one higher-order inertia term (inertia gradient). In this research we have highlighted the potentials of an enhanced format of gradient elasticity in the context of wave dispersion, which may be viewed as an extension of the latter model by incorporating *three* length scale material parameters. The relative magnitudes between these three length scales are adjusted by three coefficients that are termed α, β, γ in this paper. The γ term is associated with the Laplacian of the strain field, while the α and β coefficients multiply *two* higher-order inertia terms. As compared to the popular two length-scale gradient model, there is one more micro-inertia term (linearly proportional to the β constant) multiplying the fourth-order space derivative of the acceleration field in the equations of motion. The earlier two-length-scale model can thus be retrieved as a special case by assuming $\beta=0$.

It is rather obvious that additional gradient enrichments improve the dispersion behavior of higher-order continuum models. To demonstrate and quantify this, a set of experimental findings available in the literature and/or benchmark solutions based on micromechanics have been considered and compared to the analytical dispersion curves provided by gradient elasticity. In particular, the dispersive wave propagation in composite laminates with periodic microstructure, in metal nano-structured crystals of aluminum and bismuth, and in concrete and mortar specimens has been investigated. It has been found that there are significant improvements in the prediction of the dispersive behavior as observed in experiments and micro-mechanical data by including the additional micro-inertia term proportional to the fourth-order space derivative of the acceleration.

Since the identification and quantification of internal constitutive parameters of gradient elasticity is usually viewed as an intricate task, we have provided a few procedures by which such parameters can be linked to material microstructural properties. In composite laminates with periodic microstructure, length scale identification is carried out based on higher-order asymptotic homogenization. Moreover, length scale quantification procedures have been discussed for concrete specimens and related to the real distribution of inclusions in the underlying microstructure with the aid of a lattice model.

Another important aspect that makes the three-length-scale gradient formulation particularly appealing from a numerical point of view is concerned with the relevant finite element implementation. Application of a specific operator split to the original fourth-order differential equations with three higher-order terms results in a set of two second-order differential equations. This implies that a standard finite element implementation with linear shape functions ($\mathcal{C}^0$-continuity) is sufficient. As a result, it is concluded that the additional β term considerably improves the dispersive behavior, but at the same time it does not imply any extra computational cost as compared to the two-length-scale model with one micro-inertia and one micro-stiffness term.

Acknowledgments

The second and third authors would like to acknowledge support of the EU RISE project (FRAMED-734485) . The last author is also grateful to the Ministry of Science and Education of the Russian Federation through contract No.14.250.31.0039 which enabled the completion of the present article (25% effort).

References

Aggelis, D.G., Polyzos, D., Philippidis, T.P., 2005. Wave dispersion and attenuation in fresh mortar: theoretical predictions vs. experimental results. J. Mech. Phys. Solids 53, 857–883.
Aifantis, E.C., 1992. On the role of gradients in localization of deformation and fracture. Int. J. Eng. Sci. 30, 1279–1299.
Aifantis, E.C., 2016. Internal length gradient (ILG) material mechanics across scales and disciplines. Adv. Appl. Mech. 49, 1–110.
Altan, B., Aifantis, E.C., 1997. On some aspects in the special theory of gradient elasticity. J. Mech. Behav. Mater. 8, 231–282.
Andrianov, I.V., Awrejcewicz, J., Weichert, D., 2010. Improved continuous models for discrete media. Math. Probl. Eng., 986242 35 pages.
Andrianov, I.V., Danishevs'kyy, V.V., Topol, H., Weichert, D., 2011a. Homogenization of a 1D nonlinear dynamical problem for periodic composites. ZAMM 91 (6), 523–534.
Andrianov, I., Awrejcewicz, J., Danishevskyy, V., Weichert, D., 2011b. Wave propagation in periodic composites: Higher-order asymptotic analysis versus plane–wave expansions method. J. Comput. Nonlinear Dyn. 6 011015-1–011015-8.
Andrianov, I., Bolshakov, V., Danishevskyy, V., Weichert, D., 2008. Higher order asymptotic homogenization and wave propagation in periodic composite materials. Proc. R. Soc. A 464, 1181–1201.
Ansari, R., Gholami, R., Rouhi, H., 2012. Vibration analysis of single-walled carbon nanotubes using different gradient elasticity theories. Composites 43, 2985–2989.
Askes, H., Aifantis, E.C., 2011. Gradient elasticity in statics and dynamics: an overview of formulations, length scale identification procedures, finite element implementations and new results. Int. J. Solids Struct. 48, 1962–1990.
Askes, H., Aifantis, E.C., 2006. Gradient elasticity theories in statics and dynamics – a unification of approaches. Int. J. Fract. 139, 297–304.
Askes, H., Bennett, T., Aifantis, E.C., 2007. A new formulation and C^0-implementation of dynamically consistent gradient elasticity. Int. J. Numer. Methods Eng. 72, 111–126.
Askes, H., Metrikine, A.V., Pichugin, A., Bennett, T., 2008. Four simplified gradient elasticity models for the simulationof dispersive wave propagation. Philos. Mag. 88, 3415–3443.
Askes, H., Metrikine, A.V., 2002. One-dimensional dynamically consistent gradient elasticity models derived from a discrete microstructure. Part 2: static and dynamic response. Eur. J. Mech. 21, 573–588.
Bažant, Z.P., Jirásek, M., 2002. Nonlocal integral formulations of plasticity and damage: survey of progress. J. Eng. Mech. 11, 1119–1149.
Bedford, A., Drumheller, D.S., 1994. Introduction to Elastic Wave Propagation. Wiley, New York.

Please cite this article as: D. De Domenico et al., Gradient elasticity and dispersive wave propagation: Model motivation and length scale identification procedures in concrete and composite laminates, International Journal of Solids and Structures (2018), https://doi.org/10.1016/j.ijsolstr.2018.09.007

Bennett, T., Gitman I, M., Askes, H., 2007. Elasticity theories with higher-order gradients of inertia and stiffness for the modelling of wave dispersion in laminates. Int. J. Fract. 148, 185–193.
Carta, G., Bennett, T., Askes, H., 2012. Determination of dynamic gradient elasticity length scales. In: Proceedings of the ICE-Engineering and Computational Mechanics, 165, pp. 41–47.
Chang, C.S., Gao, J., 1995. Second-gradient constitutive theory for granular material with random packaging structure. Int. J. Solids Struct. 32, 2279–2293.
Chen, W., Fish, J., 2001. A dispersive model for wave propagation in periodic heterogeneous media based on homogenization with multiple spatial and temporal scales. J. Appl. Mech. 68, 153–161.
De Domenico, D., Askes, H., 2016. A new multi-scale dispersive gradient elasticity model with micro-inertia: formulation and C^0-finite element implementation. Int. J. Numer. Methods Eng. 108 (5), 485–512.
De Domenico, D., Askes, H., 2017. Computational aspects of a new multi-scale dispersive gradient elasticity model with micro-inertia. Int. J. Numer. Methods Eng. 109 (1), 52–72.
De Domenico, D., Fuschi, P., Pardo, S., Pisano, A.A., 2014. Strengthening of steel-reinforced concrete structural elements by externally bonded FRP sheets and evaluation of their load carrying capacity. Compos. Struct. 118, 377–384.
De Domenico, D., 2015. RC members strengthened with externally bonded FRP plates: a FE-based limit analysis approach. Composites 71, 159–174.
Donà, M., Lombardo, M., Barone, G., 2015. Experimental study of wave propagation in heterogeneous materials. In: Kruis, J, Tsompanakis, J, Topping, BHV (Eds.), Proceedings of CC2015. Prague, Czech Republic 1-4 Sept, Paper 208.
Dontsov, E.V., Tokmashev, R.D., Guzina, B.B., 2013. A physical perspective of the length scales in gradient elasticity through the prism of wave dispersion. Int. J. Solids Struct. 50, 3674–3684.
Engel, G., Garikipati, K., Hughes, T.J.R., Larson, M.G., Mazzei, L., Taylor, R.L., 2002. Continuous/discontinuous finite element approximations of fourth-order elliptic problems in structural and continuum mechanics with applications to thin beams and plates, and strain gradient elasticity. Comput. Meth. Appl. Mech. Eng. 191, 3669–3750.
Eringen, A.C., 1983. On differential equations of nonlocal elasticity and solutions of screw dislocation and surface waves. J. Appl. Phys. 54, 4703–4710.
Filimonov, A.M., 1996. Continuous approximations of difference operators. J Difference Eq. Appl. 2 (4), 411–422.
Fish, J., Chen, W., Nagai, G., 2002. Non-local dispersive model for wave propagation in heterogeneous media: one-dimensional case. Int. J. Numer. Methods Eng. 54, 331–346.
Fish, J., Chen, W., 2001. Higher-order homogenization of initial/boundary-value problem. J. Eng. Mech. 127, 1223–1230.
Fuschi, P., Pisano, A.A., De Domenico, D., 2015. Plane stress problems in nonlocal elasticity: finite element solutions with a strain-difference-based formulation. J. Math. Anal. Appl. 431, 714–736.
Hughes, T.J.R., 2000. The Finite Element Method: Linear Static and Dynamic Finite Element Analysis. Dover, NY, USA.
Iliopoulos, S.N., Aggelis, D.G., Polyzos, D., 2016. Wave dispersion in fresh and hardened concrete through the prism of gradient elasticity. Int. J. Solids Struct. 78-79, 149–159.
Jacobs, L.J., Owino, J.O., 2000. Effect of aggregate size on attenuation of Rayleigh surface waves in cement-based materials. J. Eng. Mech. ASCE 126 (11), 1124–1130.
Kim, D.S., Park, H.C., 2002. Determination of dispersive phase velocities for SASW method using harmonic wavelet transform. Soil Dyn. Earthquake Eng. 22 (8), 675–684.
Kim, Y.H., Lee, S., Kim, H.C., 1991. Attenuation and dispersion of elastic waves in multi-phase materials. J. Phys. D Appl. Phys. 24, 1722–1728.
Kinra, V.K., Petraitis, M.S., Datta, S.K., 1980. Ultrasonic wave propagation in a random particulate composite. Int. J. Solids Struct. 16, 301–312.
Madeo, A., Neff, P., Aifantis, E.C., Barbagallo, G., d'Agostino, M.V., 2017. On the role of micro-inertia in enriched continuum mechanics. Proc. R. Soc. A 473 (2198), 20160722 The Royal Society.
Malhotra, V.M., Carino, N.J., 1991. CRC Handbook on Nondestructive Testing of Concrete. CRC Press, Florida.
Maugin, G.A., Metrikine, A.V., 2010. Mechanics of Generalized Continua One Hundred Years After the Cosserats. Springer, New York.
Metrikine, A.V., Askes, H., 2006. An isotropic dynamically consistent gradient elasticity model derived from a 2D lattice. Philos. Mag. 86, 3259–3286.
Metrikine, A.V., Askes, H., 2002. One-dimensional dynamically consistent gradient elasticity models derived from a discrete microstructure. Part 1: Generic formulation. Eur. J. Mech. 21, 555–572.
Mindlin, R., 1964. Micro-structure in linear elasticity. Arch. Ration. Mech. Anal. 16, 51–78.
Papargyri-Beskou, S., Polyzos, D., Beskos, D.E., 2009. Wave dispersion in gradient elastic solids and structures: a unified treatment. Int. J. Solids Struct. 46, 3751–3759.
Philippidis, T.P., Aggelis, D.G., 2005. Experimental study of wave dispersion and attenuation in concrete. Ultrasonics 43, 584–595.
Pisano, A.A., Fuschi, P., De Domenico, D., 2014. Limit state evaluation of steel-reinforced concrete elements by von Mises and Menétrey-Willam-type yield criteria. Int. J. Appl. Mech. 6 (5), 1450051–1450058. doi:10.1142/S1758825114500586.
Pisano, A.A., Fuschi, P., De Domenico, D., 2015. Numerical limit analysis of steel-reinforced concrete walls and slabs. Comput. Struct. 160, 42–55.
Polizzotto, C., Fuschi, P., Pisano, A.A., 2006. A nonhomogeneous nonlocal elasticity model. Eur. J. Mech. A/Solids 25, 308–333.
Polyzos, D., Fotiadis, D.I., 2012. Derivation of Mindlin's first and second strain gradient elastic theory via simple lattice and continuum models. Int. J. Solids Struct. 49, 470–480.
Popovics, S., Popovics, J.S., 1998. Ultrasonic testing to determine water–cement ratio for freshly mixed concrete. Cement Concr. Aggr. 20 (2), 262–268.
Popovics, S., Rose, J.L., Popovics, J.S., 1990. The behavior of ultrasonic pulses in concrete. Cem. Concr. Res. 20, 259–270.
Ru, C.Q., Aifantis, E.C., 1993. A simple approach to solve boundary-value problems in gradient elasticity. Acta Mech. 101, 59–68.
Ruzzene, M., Baz, A., 2000. Control of wave propagation in periodic composite rods using shape memory inserts. J. Vib. Acoust. 122, 151–159.
Sachse, W., Pao, Y.-H., 1978. On the determination of phase and group velocities of dispersive waves in solids. J. Appl. Phys. 49 (8), 4320–4327.
Triantafyllidis, N., Aifantis, E.C., 1986. A gradient approach to localization of deformation. I. Hyperelastic materials. J. Elasticity 16, 225–237.
Truesdell, C., Noll, W., 2004. The non-linear field theories of mechanics. In: The Non-linear Field Theories of Mechanics. Springer, Berlin, Heidelberg, pp. 1–579.
Truesdell, C., Toupin, R., 1960. The classical field theories. In: Principles of Classical Mechanics and Field Theory/Prinzipien Der Klassischen Mechanik Und Feldtheorie. Springer, Berlin, Heidelberg, pp. 226–858.
Warren, J., Yarnell, J., Dolling, G., Cowley, R., 1967. Lattice dynamics of diamond. Phys. Rev. 158, 805–808.
Yarnell, J., Warren, J., Koenig, S., 1965. Experimental dispersion curves for phonons in aluminium. In: Wallis, RF (Ed.), Lattice Dynamics – Proceedings of An International Conference. Pergamon Press, Oxford (UK), pp. 57–61.
Yarnell, J., Warren, J., Wenzel, R., Koenig, S., 1964a. Phonon dispersion curves in bismuth. IBM J. Res. Dev. 8, 234–240.
Yarnell, J., Warren, J., Wenzel, R., 1964b. Lattice vibrations in diamond. Phys. Rev. Lett. 13, 13–15.
Ye, G., vanBreugel, K., Fraij, A.L.A., 2003. Experimental study and numerical simulation on the formation of microstructure in cementitious materials at early age. Cem. Concr. Res. 33, 233–239.
Zervos, A., Papanicolopulos, S.A., Vardoulakis, I., 2009. Two finite element discretizations for gradient elasticity. J. Eng. Mech. 135, 203–213.
Zervos, A., 2008. Finite elements for elasticity with microstructure and gradient elasticity. Int. J. Numer. Methods Eng. 73, 564–595.

Please cite this article as: D. De Domenico et al., Gradient elasticity and dispersive wave propagation: Model motivation and length scale identification procedures in concrete and composite laminates, International Journal of Solids and Structures (2018), https://doi.org/10.1016/j.ijsolstr.2018.09.007